Modulation of interphase, cross-scale momentum transfer of turbulent flows by preferentially concentrated inertial particles

Miralireza Nabavi [1], Mario Di Renzo [2], and Jeonglae Kim [1,*]
[1] *School for Engineering of Matter, Transport and Energy, Arizona State University, Tempe, Arizona 85287, USA*
[2] *Centre Européen de Recherche et de Formation Avancée en Calcul Scientifique, Toulouse, France*

(Received 31 October 2021; accepted 14 April 2022; published 27 April 2022)

Wavelet multiresolution analysis is extended to describe interphase, cross-scale interactions involving turbulence kinetic energy (TKE) of particle-laden turbulence. Homogeneous isotropic turbulence (HIT) suspended with inertial particles at the Stokes number of unity (critical particles) is analyzed. Direct numerical simulation is performed for decaying HIT coupled via the Stokes drag law in two ways with the dispersed phase. The effects of two-way coupling on spectral TKE transfer are examined. Clustering of the critical particles in thin, filamentlike regions is observed, and mean wavelet statistics are similar to those of the Fourier analysis. However, spatially local wavelet analysis demonstrates the complexities of the preferential concentration in interphase, interscale energy transfer and associated challenges in subgrid-scale (SGS) modeling of particle-laden turbulence. Two-way coupling enhances correlations between local particle concentration and local interphase TKE transfer. However, particle concentration alone does not indicate a definite direction of interphase energy transfer. Rather, particle clusters behave as an energy source or sink with similar probabilities. A similar argument is made for correlations between particle concentration and cross-scale energy transfer. Wavelet statistics conditioned on coarse-grained number density support the same conclusions. In addition, the joint statistics show the qualitative consistency of the SGS Stokes number in describing the two-way interactions, which should be considered in the SGS modeling of two-way coupled particle-laden turbulence.

DOI: 10.1103/PhysRevFluids.7.044305

I. INTRODUCTION

Particle-laden flows are widely encountered in nature and various engineering applications [1–4]. Understanding and modeling particle dispersion is relevant to some of the environmental, public health, ecological, and climate concerns involving pollutant particles [5], plume formation in the atmosphere [6], plankton accumulation in the oceans [7], and airborne spreading of germs and virus particles [8]. Moreover, the performance of engineering fluid systems often depends critically on how particles interact with flows in applications such as sediment prevention in pipelines [9] and the design of fuel injection systems [10]. Particles having negligible inertia (compared with the carrier-phase fluid) such as tracer particles, nanoplastics, and virus particles are advected by local fluid motions, while larger and/or heavier particles often result in complex interactions with fluid flows in mass, momentum, and energy transports. Depending on the particle mass loading ratio, such interactions may occur not only in a way that the carrier phase modifies the dispersed phase, but also in the opposite direction.

*Corresponding author: jeokim@asu.edu

Interactions of particles with the carrier phase in turbulent states are of particular interest. The multiscale and nonequilibrium nature of turbulence makes a simple mechanistic description of such interactions less straightforward. Particles respond selectively to a range of spatial and temporal scales of turbulent motions and vice versa. For instance, particles having their relaxation time comparable to the Kolmogorov timescale avoid high-vorticity regions and accumulate at a high concentration where the local strain rate is significant, known as the preferential concentration [1,11].

In simulating particle-laden turbulence, direct numerical simulation (DNS) has become a feasible tool for not only the Lagrangian point-particle approaches but also the particle-resolved simulations [12,13]. However, resolving the entire scales of fluid motions at high Reynolds numbers is still overwhelming in computational cost, and alternative approaches such as large-eddy simulation (LES) are desired. In LES, the energy-containing carrier-phase motions are predicted and the effects of unresolved small-scale fluctuations are modeled. Existing LES formulations of particle-laden turbulence are developed mainly for one-way coupled regimes where the particle mass loading is small. In general, the formulations are classified, based on how the subgrid-scale (SGS) velocity is estimated, into several categories, namely a stochastic model, approximate deconvolution, kinematic simulation, and spectrally optimized interpolation [14,15].

Fidelity of LES prediction depends strongly on modeling unresolved, SGS stresses estimated using resolved, large-scale flow motions [16]. For LES of turbulent flows laden with inertial particles, additional modeling challenges arise [1,14,17]. LES filter size is generally much larger than the Kolmogorov lengthscale, which often exceeds, even at high Reynolds numbers, the characteristic size of inertial particles. Thus, interphase interactions in LES prediction may involve unresolved flow motions, their impacts on particle dispersion, and SGS-dispersed particle forces, which in turn modify resolved-scale eddies. Such interactions can be characterized by nondimensional parameters such as the particle mass loading and SGS Stokes number [17]. Following Urzay *et al.* [17], the SGS Stokes number $\mathrm{St}_{\mathrm{SGS}}$ is introduced based on dimensional arguments, namely $\mathrm{St}_{\mathrm{SGS}} = t_{\mathrm{a}}/t_{\Delta}$, where $t_{\Delta} = (\ell_{\Delta}^2/\epsilon)^{1/3}$ is the cutoff timescale, with ℓ_{Δ} being a nominal LES filter size and t_{a} is the particle acceleration time. For instance, the mass-loading ratio of $O(1)$ and vanishingly small SGS Stokes number are associated with loaded SGS motions as such particles slip with respect to SGS eddies and behave as tracers with respect to resolved eddies. On the other hand, a large SGS Stokes number leads to particle slippage with respect to large eddies and thus a stronger modulation of resolved-scale motions (SGS unloaded). This calls for supplementary SGS models that take into account such (at least) two-way interactions and vanish in the one-way coupled regimes. In addressing the modeling challenges, describing interphase and interscale interactions (involving unresolved scales and SGS-dispersed particles) is useful. Such information can be used to develop and validate accurate SGS models for two-way coupled particle-laden turbulence.

A common analysis framework in studying turbulence modulation by inertial particles is based on the Fourier transform [18–21]. However, its advantage in having excellent spectral resolution is compromised by a complete loss of information about position. This is not desirable for particle-laden turbulence where inertial particles often respond to turbulent motions in a way that is inhomogeneous and localized [1], such as clustering, sedimentation, and turbophoresis. These difficulties can be alleviated by employing wavelet analysis. Wavelet has been employed to analyze and simulate turbulent flows [22–24]. Using wavelet, coherent flow structures can be extracted, and intermittency in turbulent flows can be estimated [25–27]. In addition, Meneveau [28] developed a formulation that evaluates multiscale energy transfer caused by the triadic interactions using orthogonal wavelet transform [29]. Similar formulations are employed and extended to turbulent channel flows [30], turbulent combustion [31], and droplet-laden turbulence [32].

For particle-laden turbulence, Bassenne *et al.* [33] developed a wavelet multiresolution analysis (WMRA) framework. For one-way coupled configurations, they analyzed both carrier- and dispersed-phase fields using WMRA, and the preferential concentration at the critical Stokes number ($\mathrm{St}_k = t_{\mathrm{a}}/t_k = 1$, where t_{a} is the particle acceleration timescale defined in Sec. II, and t_k is the Kolmogorov timescale) is characterized. However, studying turbulence modulation by inertial

particles requires a further extension of the WMRA framework to explicitly take into account the interphase and cross-scale transfer of turbulence kinetic energy (TKE).

This study extends the WMRA framework proposed by Bassenne *et al.* [33] to describe interphase and cross-scale interactions involving TKE. Interphase interactions have been analyzed in the Fourier context (Ferrante and Elghobashi [19], for example). However, its poor spatial resolution makes it inadequate to study particle-laden turbulence exhibiting strong spatial locality (such as the preferential concentration), which this study addresses using a wavelet technique. This study also examines the interscale transfer of TKE and characterizes simultaneously both interphase and interscale transfer. Spectral kinetic energy transport of two-way coupled decaying homogeneous isotropic turbulence (HIT) in a triply periodic box is evaluated as a function of scale and position in a way similar to Kim *et al.* [31], which is based on the work of Meneveau [28]. Interphase contributions to spectral kinetic energy and their correlations with local particle concentration and local subfilter-scale energy transfer due to the triadic interactions are examined using joint wavelet statistics. Decaying HIT without particles and with particles at the initial Stokes numbers of unity and 10 are investigated. Conclusions made by this study have implications for analyzing and developing SGS models for particle-laden turbulent flows in a context discussed by Urzay *et al.* [17] using a dimensional argument which this study confirms using conditional statistics.

This paper is organized as follows. The DNS governing equations and simulation details are presented in Sec. II. The wavelet multiresolution analysis framework is briefly discussed in Sec. III. Section IV describes unconditioned wavelet statistics including energy spectra and spectral energy fluxes. Conditioned wavelet statistics are discussed in Sec. V, followed by conclusions and suggested future works in Sec. VI.

II. DIRECT NUMERICAL SIMULATION OF TWO-WAY COUPLED PARTICLE-LADEN TURBULENCE

Decaying incompressible HIT suspended with inertial point particles is simulated. DNS is performed in a cubic, triply periodic computational domain of a side length $L = 2\pi$ in the Cartesian coordinates decomposed by $N^3 = 256^3$ control volumes. The continuity and momentum equations for the carrier phase are solved directly,

$$\frac{\partial u_i}{\partial x_i} = 0, \tag{1}$$

$$\frac{\partial u_i}{\partial t} + u_j \frac{\partial u_i}{\partial x_j} = -\frac{1}{\rho}\frac{\partial p}{\partial x_i} + \nu \frac{\partial^2 u_i}{\partial x_j \partial x_j} + f_i, \tag{2}$$

where u_i is a velocity component ($i = 1, 2, 3$) of the carrier-phase fluid, p is the hydrodynamic pressure, ρ is the mass density of fluid, ν is the kinematic viscosity, and f_i is the interphase coupling force in the x_i direction applied by particles to the fluid phase. Gravity is ignored in this study. Variables are made dimensionless in the same way as in Ref. [33]. A second-order central finite difference is used for spatial discretization of the carrier phase, and time advancement is fourth-order accurate [34].

The velocity field is initialized to be solenoidal and isotropic, using a prescribed Passot-Pouquet kinetic-energy model spectrum [35,36]. Forced HIT with one-way coupled particles is then allowed to evolve in order to generate an initial condition of two-way coupled simulations. The flow is forced in order to achieve statistically steady homogeneous and isotropic turbulence where a constant dissipation rate $\epsilon = \nu\langle \frac{\partial u_i}{\partial x_j}\frac{\partial u_i}{\partial x_j}\rangle = \epsilon_0$ is maintained [36]. The Reynolds number based on the Taylor microscale λ is $\mathrm{Re}_\lambda = u_\ell \lambda/\nu = 85$, where u_ℓ is the integral velocity (also the root mean square of the fluctuating velocity). Spatial resolution is $\kappa_{\max}\ell_k = 1.6$, where $\kappa_{\max} = \pi/\Delta$ is the maximum wave number, $\Delta = L/N$ is the grid spacing, and ℓ_k is the Kolmogorov lengthscale.

A total of $N_\mathrm{p} = 84 \times 10^6$ inertial particles are seeded randomly across the computational domain at $t = 0$ and dispersed by turbulence in one way. Then, the interphase coupling term is activated at

$t = t_0$, and the hydrodynamic forcing used to sustain turbulence is turned off, allowing turbulence to decay over time. The decaying particle-laden turbulence is time-advanced for $\Delta t = t - t_0 = 0.64 t_\ell$ (or $13.4 t_k$), where t_ℓ and t_k are the integral and the Kolmogorov timescales, respectively, before the two-way coupling is activated. Both flow and particle snapshots are stored every $3.35 t_k$, and a total of five snapshots are analyzed in this study. Particles are assumed spherical, and the mean particle-number density is $n_0 = N_\mathrm{p}/L^3 = 5/\Delta^3$. Particles considered in this study are much smaller than the smallest turbulent eddies in such a way that $a_\mathrm{p}/\ell_k \ll 1$, where a_p is the radius of a particle. The particle density ρ_p is much larger than the fluid density ($\rho_\mathrm{p}/\rho = 10^3$). The characteristic Reynolds number of the relative flow motion around particles is small, that is, $\mathrm{Re}_\mathrm{p} = u_k a_\mathrm{p}/\nu \ll 1$, where u_k is the Kolmogorov velocity. Thus, the viscous force acting on particles is only the Stokes drag [11]. A correction based on the local volume fraction can be made following, for instance, Tenneti *et al.* [37]. However, the particle Reynolds number and local volume fractions much less than unity justify the use of the Stokes drag model only. With the particle mass fraction ratio $\alpha = 4\pi\rho_\mathrm{p} n_0 a_\mathrm{p}^3/(3\rho) = 1$, the dispersed phase is coupled tightly with the carrier phase via f_i in Eq. (2), which is the Stokes drag force in the x_i direction exerted by particles on the carrier phase,

$$f_i = \mathcal{P}\left[\frac{u_{\mathrm{p},i} - \mathcal{I}(u_i)}{t_\mathrm{a}}\right], \tag{3}$$

where $u_{\mathrm{p},i}$ is the instantaneous velocity of the pth particle in the x_i direction, $\mathcal{I}$ is the interpolation operator from the carrier phase to the position of particles, $\mathcal{P}$ is the projection operator from particles to the computational cell center [34], and $t_\mathrm{a} = (2/9)(\rho_\mathrm{p}/\rho)(a_\mathrm{p}^2/\nu)$ is the particle acceleration time. Both interpolation and projection operators are trilinear in space. Particle volume fraction is much lower than unity, and particle-particle collision effects are ignored.

The motion of the dispersed phase is described using a Lagrangian formulation where the trajectory equation

$$\frac{dx_{\mathrm{p},i}}{dt} = u_{\mathrm{p},i}, \quad p = 1, \ldots, N_\mathrm{p}, \tag{4}$$

and the momentum conservation equation [11]

$$\frac{du_{\mathrm{p},i}}{dt} = -\frac{u_{\mathrm{p},i} - \mathcal{I}(u_i)}{t_\mathrm{a}}, \quad p = 1, \ldots, N_\mathrm{p}, \tag{5}$$

are integrated in time, where $x_{\mathrm{p},i}$ is the instantaneous position of the pth particle in the x_i direction. For the coupled wavelet analysis of the carrier and dispersed phases, particle-number density field is estimated using a trilinear projection in space [34]. The nearest-neighbor projection [33] results in nearly identical conclusions.

Particle inertia is characterized by the initial Stokes number $\mathrm{St}_{k,0} = t_\mathrm{a}/t_k$ defined when the two-way coupling is activated at $t = t_0$. Two values of the Stokes number are considered, namely $\mathrm{St}_{k,0} = 1$ and 10. At $\mathrm{St}_{k,0} = 1$, the flow and the particle characteristic timescales compete, and particles are transported by large eddies and partially slip with respect to the Kolmogorov eddies. In this way, particles tend to accumulate in ligaments located in high-strain regions formed between small eddies [17], a phenomenon known as preferential concentration [1]. On the other hand, particles are ballistic at $\mathrm{St}_{k,0} = 10$ with respect to smaller eddies, reducing the effects of the preferential concentration. Figure 1 shows instantaneous snapshots of inertial particles contained in a slab of thickness ℓ_k. The preferential concentration of $\mathrm{St}_{k,0} = 1$ particles is shown in Fig. 1(a), whereas $\mathrm{St}_{k,0} = 10$ particles are dispersed more uniformly in space as shown in Fig. 1(b).

III. WAVELET MULTIRESOLUTION ANALYSIS OF SPECTRAL ENERGY TRANSFER IN TWO-WAY COUPLED PARTICLE-LADEN TURBULENCE

The wavelet formulation is based on the work of Bassenne *et al.* [33] for one-way coupled particle-laden turbulence, which is similar to the work of Meneveau [28] for single-phase,

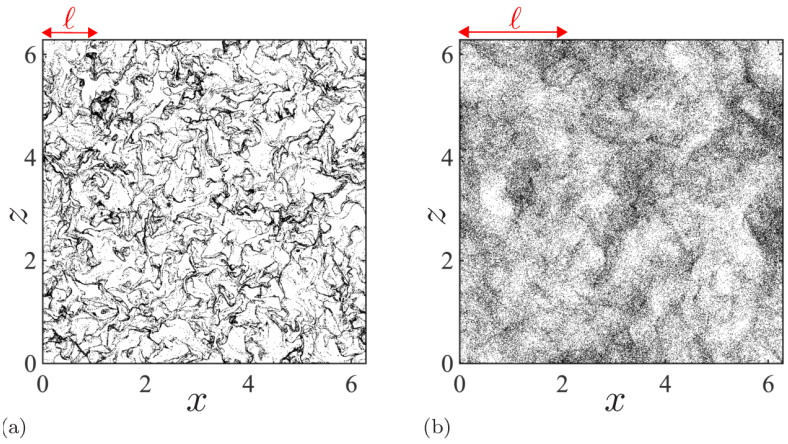

FIG. 1. Instantaneous particle distributions at $\Delta t/t_\ell = 0.64$ on an x-z cross section of thickness equal to ℓ_k for $\mathrm{St}_{k,0}$ = (a) 1 and (b) 10. The arrows denote the integral lengthscales ℓ (to scale).

incompressible turbulent flows. This study extends the formulation of Bassenne *et al.* [33] to include the interphase and interscale energy transfer, with which an analysis framework is proposed for two-way coupled particle-laden turbulence and its LES. The current work is distinguished from the other wavelet formulations examining multiscale interactions [28,30–32,38] in that interphase interactions are directly incorporated and analyzed simultaneously with interscale interactions to study the two-way interactions between fluid and particle phases.

Consider a three-dimensional scalar field $C[\boldsymbol{x}_0]$ (for instance, number density n or a componentwise velocity u_i) defined at the cell centers of a computational grid with uniform spacing Δ and a number of control volumes N along a direction,

$$\boldsymbol{x}_0 = (i\Delta/2,\, j\Delta/2,\, k\Delta/2), \tag{6}$$

where $i = 1, 3, 5, \ldots, 2N-1$, $j = 1, 3, 5, \ldots, 2N-1$, and $k = 1, 3, 5, \ldots, 2N-1$. For brevity, dependence on time t is suppressed. Three-dimensional discrete wavelet series expansion of $C[\boldsymbol{x}_0]$ in a triply periodic domain is given by

$$\begin{aligned} C[\boldsymbol{x}_0] &= \sum_{s=1}^{\mathcal{S}} \sum_{\boldsymbol{x}_s} \sum_{d=1}^{7} \check{C}^{(s,d)}[\boldsymbol{x}_s]\mathcal{G}^{(s,d)}[\boldsymbol{x}_0 - \boldsymbol{x}_s] + \sum_{\boldsymbol{x}_\mathcal{S}} \widehat{C}^{(\mathcal{S})}[\boldsymbol{x}_\mathcal{S}]\mathcal{H}^{(\mathcal{S})}[\boldsymbol{x}_0 - \boldsymbol{x}_\mathcal{S}] \\ &= \sum_{s=1}^{\mathcal{S}} C^{(s)}[\boldsymbol{x}_0] + \sum_{\boldsymbol{x}_\mathcal{S}} \widehat{C}^{(\mathcal{S})}[\boldsymbol{x}_\mathcal{S}]\mathcal{H}^{(\mathcal{S})}[\boldsymbol{x}_0 - \boldsymbol{x}_\mathcal{S}], \end{aligned} \tag{7}$$

where $s = 1, 2, \ldots, \mathcal{S}$ is the scale index, with $\mathcal{S} = \log_2 N = 8$ being the maximum resolution supported by the present data, and $d = 1, 2, \ldots, 7$ is the directionality index. In (7), $\mathcal{G}^{(s,d)}[\boldsymbol{x}_0 - \boldsymbol{x}_s]$ and $\mathcal{H}^{(\mathcal{S})}[\boldsymbol{x}_0 - \boldsymbol{x}_\mathcal{S}]$ correspond to a three-dimensional discrete wavelet basis and scaling function obtained by a tensor product of a one-dimensional wavelet basis and scaling function (for instance, those of Haar, Daubechies, and Coifman), respectively. The discrete wavelet coefficient is evaluated as

$$\check{C}^{(s,d)}[\boldsymbol{x}_s] = \langle C[\boldsymbol{x}_0]\mathcal{G}^{(s,d)}[\boldsymbol{x}_0 - \boldsymbol{x}_s]\rangle \tag{8}$$

by invoking the orthogonality conditions

$$\langle \mathcal{G}^{(s,d)}[\boldsymbol{x}_0 - \boldsymbol{x}_s]\mathcal{G}^{(s',d')}[\boldsymbol{x}_0 - \boldsymbol{x}_{s'}]\rangle = \delta_{s,s'}\delta_{d,d'}\delta_{\boldsymbol{x}_s,\boldsymbol{x}_{s'}} \tag{9}$$

and

$$\langle \mathcal{G}^{(s,d)}[\boldsymbol{x}_0 - \boldsymbol{x}_s]\mathcal{H}^{(\mathcal{S})}[\boldsymbol{x}_0 - \boldsymbol{x}_\mathcal{S}]\rangle = 0, \tag{10}$$

where δ_{ij} is the Kronecker delta and $\langle\,\rangle = (1/N^3)\sum$ denotes the volume average operator on the DNS grid. The wavelet coefficient at scale s is defined at the dyadic grid points $\boldsymbol{x}_s = 2^{s-1}(i\Delta, j\Delta, k\Delta)$, where $i = 1, 3, 5, \ldots, N/2^{s-1} - 1$, $j = 1, 3, 5, \ldots, N/2^{s-1} - 1$, and $k = 1, 3, 5, \ldots, N/2^{s-1} - 1$. As the scale index increases, the number of points in the wavelet grid decreases by a factor of $2^3 = 8$. For instance, the present DNS grid contains $N^3 \approx 16.8$ million points, and the wavelet grid at the maximum scale $\mathcal{S} = 8$ has a single point. Scale-dependent wavelet grid spacing is defined by $\ell_s = 2^s\Delta$ with $\ell_1 = 2\Delta$ and $\ell_8 = L$, corresponding to the smallest and largest lengthscales, respectively. A representative wave number is defined by

$$\kappa = \frac{2\pi}{\ell_s} = \frac{2\pi}{2^s\Delta}, \tag{11}$$

from which the spectral resolution is obtained as

$$\delta\kappa = \frac{2\pi\,\ln 2}{\ell_s} = \kappa\,\ln 2. \tag{12}$$

Alternatively, Eq. (11) can be defined as a centroid wave number of the wavelet basis used in the analysis, giving an additional constant prefactor [23]. It is noted that the spectral resolution is proportional to the wave number itself, indicating that smaller scales are associated with poorer spectral resolution. This is in contrast to spatial resolution, which becomes poorer at larger scales. As a consequence, excellent spatial resolution does not achieve excellent spectral resolution simultaneously, known as the uncertainty principle [39]. In this study, as inertial particles at the critical Stokes number ($\mathrm{St}_{k,0} = 1$) concentrate preferentially within very narrow regions in space, excellent spatial resolution is desired. The simplest Haar wavelet offers the best spatial localization at the cost of the largest spectral leakage [39]. For instance, the family of the Coifman wavelet basis reduces the spectral leakage as its number of vanishing moments increases. However, its statistics become increasingly nonlocal in space, partially losing the benefits of employing wavelet decomposition. In this study, the 24-point Coifman basis is applied to compute wavelet statistics. In Sec. V, the Haar basis is also employed for its excellent spatial localization, which is useful for correlating statistics with a scale-dependent particle concentration.

Following Bassenne *et al.* [33], the local wavelet spectrum of turbulence kinetic energy (TKE), $k = \frac{1}{2}u_iu_i$, is defined as

$$\check{E}[\kappa, \boldsymbol{x}_s] = \frac{2^{-3s}}{\delta\kappa}\sum_{d=1}^{7}\check{u}_i^{(s,d)}[\boldsymbol{x}_s]\check{u}_i^{(s,d)}[\boldsymbol{x}_s]. \tag{13}$$

The mean wavelet energy spectrum per scale is given by

$$\check{E}[\kappa] = \langle\check{E}[\kappa, \boldsymbol{x}_s]\rangle_{\boldsymbol{x}_s}, \tag{14}$$

where $\langle\,\rangle_{\boldsymbol{x}_s} = (2^{3s}/N^3)\sum_{\boldsymbol{x}_s}$ denotes the average over the wavelet-colocation grid at scale s, which provides scale-dependent mean wavelet statistics. In general, the mean wavelet spectrum Eq. (14) converges to the Fourier energy spectrum as the wavelet basis has more vanishing moments. Following Meneveau [28], the discrete wavelet transform is applied to Eq. (2), and the transport equation of the wavelet energy spectrum is obtained as

$$\frac{\partial\check{E}[\kappa, \boldsymbol{x}_s]}{\partial t} = \check{T}_\mathrm{C}[\kappa, \boldsymbol{x}_s] + \check{T}_\mathrm{P}[\kappa, \boldsymbol{x}_s] + \check{T}_\mathrm{V}[\kappa, \boldsymbol{x}_s] + \check{T}_\psi[\kappa, \boldsymbol{x}_s], \tag{15}$$

where

$$\check{T}_{\mathrm{C}}[\kappa,\boldsymbol{x}_s] = -\frac{2^{-3s}}{\delta\kappa}\sum_{d=1}^{7}\check{u}_i^{(s,d)}[\boldsymbol{x}_s]u_j\frac{\check{\partial}u_i}{\partial x_j}^{(s,d)}[\boldsymbol{x}_s], \tag{16}$$

$$\check{T}_{\mathrm{P}}[\kappa,\boldsymbol{x}_s] = -\frac{2^{-3s}}{\delta\kappa}\sum_{d=1}^{7}\check{u}_i^{(s,d)}[\boldsymbol{x}_s]\frac{1}{\rho}\frac{\check{\partial}p}{\partial x_i}^{(s,d)}[\boldsymbol{x}_s], \tag{17}$$

$$\check{T}_{\mathrm{V}}[\kappa,\boldsymbol{x}_s] = \frac{2^{-3s}}{\delta\kappa}\sum_{d=1}^{7}\check{u}_i^{(s,d)}[\boldsymbol{x}_s]\nu\frac{\check{\partial}^2u_i}{\partial x_j\partial x_j}^{(s,d)}[\boldsymbol{x}_s], \tag{18}$$

$$\check{T}_{\psi}[\kappa,\boldsymbol{x}_s] = \frac{2^{-3s}}{\delta\kappa}\sum_{d=1}^{7}\check{u}_i^{(s,d)}[\boldsymbol{x}_s]\check{f}_i^{(s,d)}[\boldsymbol{x}_s], \tag{19}$$

represent spectral kinetic energy fluxes due to the convective, pressure, viscous transports, and particle drag force, respectively. The mean energy fluxes are defined in a way similar to Eq. (14) (for instance, $\check{T}_{\psi}[\kappa] = \langle\check{T}_{\psi}[\kappa,\boldsymbol{x}_s]\rangle_{\boldsymbol{x}_s}$). Summing the fluxes over all scales and locations recovers the global energy balance in a triply periodic domain,

$$\frac{d\langle k\rangle}{dt} = -\epsilon + \psi, \tag{20}$$

where $\psi = \alpha\langle u_i f_i\rangle$ is the volume-averaged rate of energy change due to the particle drag force, with α being the mass-loading ratio defined in Sec. II.

For understanding spectral energy transfer, it is useful to quantify how much TKE is transported from large to small scales and vice versa. Following Meneveau [28], a velocity field is decomposed into components smaller and larger than a cutoff scale n, namely

$$u_i[\boldsymbol{x}_0] = u_i^{<n}[\boldsymbol{x}_0] + u_i^{>n}[\boldsymbol{x}_0] = \sum_{s=1}^{n-1}u_i^{(s)}[\boldsymbol{x}_0] + \sum_{s=n}^{\mathcal{S}}u_i^{(s)}[\boldsymbol{x}_0]. \tag{21}$$

A similar decomposition can be applied to other variables such as pressure and number density. In particular, this decomposition is used to unambiguously evaluate the cross-scale convective energy transfer (across the cutoff scale n) via

$$\frac{\partial}{\partial x_j}(u_iu_j) = \frac{\partial}{\partial x_j}\left(u_iu_j - u_i^{>n}u_j^{>n}\right) + \frac{\partial}{\partial x_j}\left(u_i^{>n}u_j^{>n}\right). \tag{22}$$

The last term represents interactions involving scales larger than n only. By excluding this superfilter-scale interaction, the cross-scale convective transfer across a cutoff scale n is obtained. This is done by introducing the detailed energy transfer involving convective and pressure transports between a scale m and all scales smaller than the cutoff scale n,

$$\check{T}_{\mathrm{CP}}[\kappa_m|\kappa_n,\boldsymbol{x}_m] = \sum_{i=1}^{3}\sum_{d=1}^{7}\check{u}_i^{(m,d)}[\boldsymbol{x}_m]\left\{\frac{\partial}{\partial x_j}\left(u_iu_j - \check{u_i^{>n}u_j^{>n}}\right) + \frac{1}{\rho}\frac{\partial}{\partial x_i}p^{<n}\right\}^{(m,d)}[\boldsymbol{x}_m]. \tag{23}$$

Integrating $\check{T}_{\mathrm{CP}}$ over scales larger than the cutoff scale n gives the cumulative detailed energy flux due to convective and pressure transports. This quantifies the rate at which TKE is transferred from larger scales to scales smaller than n via the triadic interactions, namely

$$\Pi_{\mathrm{SFS}}[\kappa_n,\boldsymbol{x}_n] = -\sum_{m=n}^{\mathcal{S}}2^{-3(m-\mathcal{S})}\check{T}_{\mathrm{CP}}[\kappa_m|\kappa_n,\boldsymbol{x}_m]. \tag{24}$$

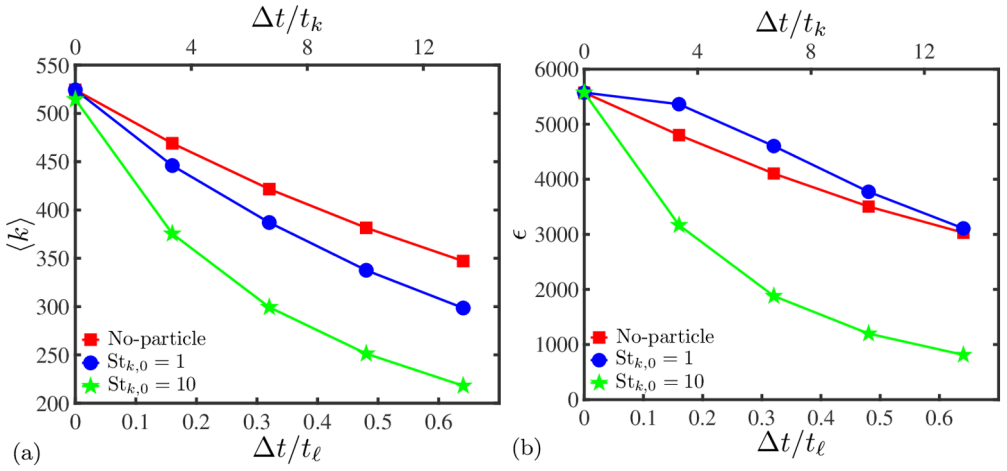

FIG. 2. Time development of (a) volume-averaged TKE and (b) viscous dissipation rate.

This cumulative subfilter-scale (SFS) flux is volumed-averaged over the wavelet colocation grid to obtain the mean cumulative SFS flux $\Pi_{\mathrm{SFS}}[\kappa]$, similar to Eq. (14). The same SFS flux is used to study energy backscatter in homogeneous isotropic turbulence and homogeneously sheared flow [28].

IV. UNCONDITIONED STATISTICS

A. Volume-averaged statistics

Figure 2(a) shows the decay of volume-averaged TKE. Consistent with the literature for point particles at $\mathrm{St}_{k,0} \geqslant 1$ [19,40,41], TKE is reduced much more rapidly as particle inertia increases. A similar observation is made for the viscous dissipation rate plotted in Fig. 2(b). Note that for $\mathrm{St}_{k,0} = 1$, the dissipation rate stays close to ϵ_0 during the initial $0.16t_\ell$. In Fig. 3, instantaneous Stokes numbers are estimated using the instantaneous dissipation rates shown in Fig. 2(b). They are normalized by the initial Stokes numbers $\mathrm{St}_{k,0} = 1$ and 10, respectively. For $\mathrm{St}_{k,0} = 1$, the Stokes number decays by 20% for $0.64t_\ell$, while the relative decay is three times larger for $\mathrm{St}_{k,0} = 10$.

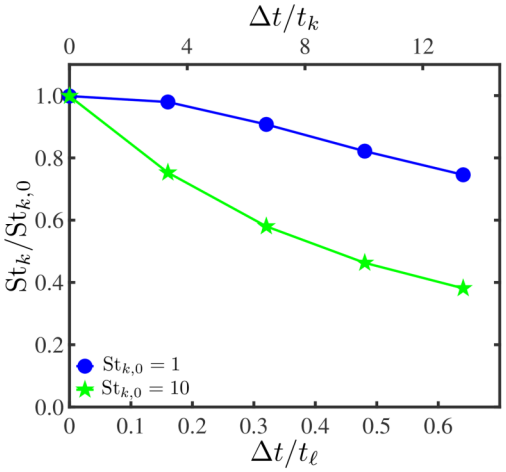

FIG. 3. Normalized Stokes numbers estimated using instantaneous volume-averaged statistics.

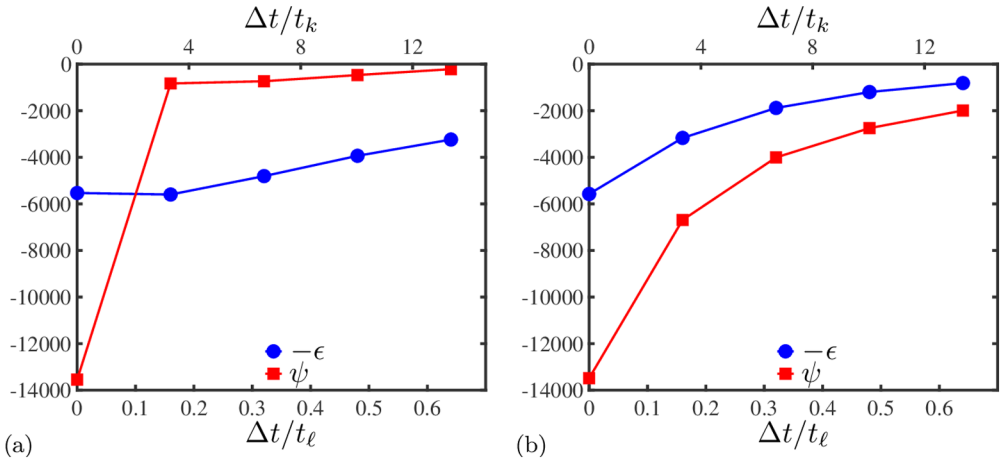

FIG. 4. Dissipation rate and interphase energy exchange due to the particle drag force for $\mathrm{St}_{k,0} =$ (a) 1 and (b) 10.

However, it is noteworthy that the $\mathrm{St}_{k,0} = 10$ particles remain in heavy particle regimes for the entire duration of the calculation even after such a decay. As shown in Fig. 4, particles attenuate a substantial amount of TKE for both Stokes numbers at least during the initial phase ($\Delta t/t_k \lesssim 3$) of two-way coupled simulations. Work done by the critical particles [Fig. 4(a)] quickly decays and stays much smaller in magnitude than that by heavy particles [Fig. 4(b)]. For $\mathrm{St}_{k,0} = 1$, the viscous mechanisms dominate in dissipating TKE at $\Delta t/t_\ell \gtrsim 0.16$ [Fig. 4(a)] as the critical particles are accumulated within very narrow regions between eddies, whereas ψ remains always larger in magnitude than ϵ for $\mathrm{St}_{k,0} = 10$ [Fig. 4(b)]. Observations reported in this section are consistent with the well-documented modulations of volume-averaged statistics as a function of Stokes number for two-way coupled decaying HIT laden with point particles [19,41].

B. Mean wavelet statistics

Mean wavelet statistics show Stokes-number dependence in agreement with the Fourier analysis of two-way coupled HIT [19,40,41]. Figure 5(a) compares the mean wavelet energy spectra at $\Delta t/t_\ell = 0.64$. For $\mathrm{St}_{k,0} = 1$, TKE increases at high wave numbers and decreases at small wave

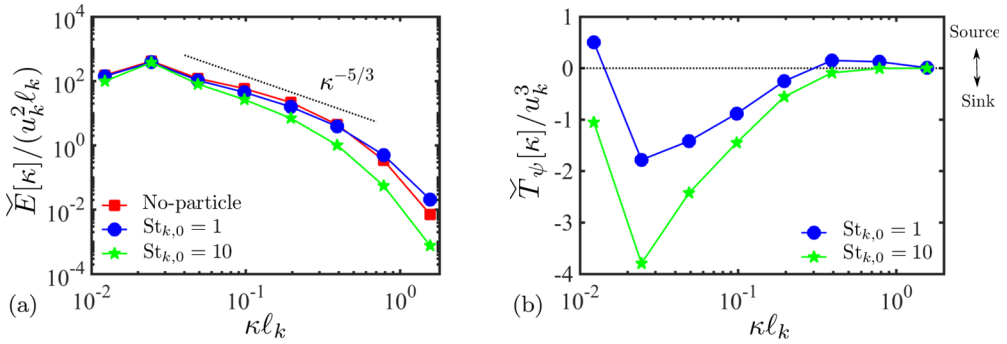

FIG. 5. Comparison of (a) the mean wavelet spectra of TKE and (b) the mean spectral energy transfer due to the particle drag force at $\Delta t/t_\ell = 0.64$. In (b), the horizontal dotted line denotes the neutral interphase transfer.

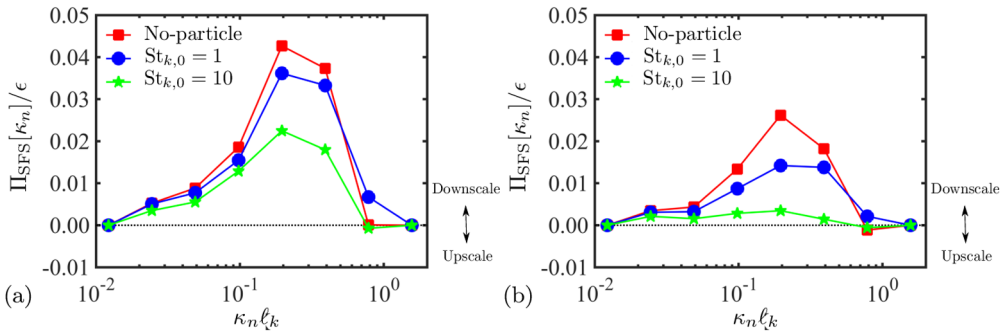

FIG. 6. Mean cumulative energy fluxes due to convective and pressure transports at (a) $\Delta t/t_\ell = 0.16$ and (b) $\Delta t/t_\ell = 0.64$. The horizontal dotted lines denote the in-scale transfer.

numbers compared with the particle-free simulation. On the other hand, TKE is reduced across all scales for $\mathrm{St}_{k,0} = 10$. Two-way interacting particles increase intermittency estimated by the flatness factors of energy and enstrophy spectra at small scales compared with the particle-free simulation (not shown).

Scale-dependent contributions of inertial particles to TKE are analyzed by computing mean spectral energy transfer due to the drag force, as done previously using the Fourier analysis [19,41]. Figure 5(b) shows that while heavy particles ($\mathrm{St}_{k,0} = 10$) dissipate TKE on average across all scales, the critical particles ($\mathrm{St}_{k,0} = 1$) provide a net positive increase of TKE at $\kappa \ell_k \gtrsim 0.3$. Similar to the observations made using the Fourier analysis [19,40], the critical point particles attenuate energy contained in large turbulent motions and energize small-scale eddies on average, while heavy point particles behave as a consistent sink of TKE. The maximum attenuation due to the interphase force is much larger for heavy particles due to their ballistic behaviors and slippage with respect to larger eddies. The critical particles tend to cluster within narrow zones confined by strong vortical motions, and their direct contributions to large scales where they behave as tracers are limited. Wavelet energy spectra and fluxes at times other than $\Delta t/t_\ell = 0.64$ are similar and thus not shown in this manuscript.

To characterize the effects of particle inertia on the spectral energy transfer of the carrier-phase turbulence, the mean cross-scale energy transfer defined in Eq. (24) is shown in Fig. 6. By definition, $\Pi_{\mathrm{SFS}}[\kappa_1] = 0$ since the cutoff scale $n = 1$ has no subfilter scale, and $\Pi_{\mathrm{SFS}}[\kappa_8] = 0$ since there is no scale larger than $n = 8$ in the present setup. All three cases show similar trends at both $\Delta t/t_\ell = 0.16$ and 0.64, namely net positive downscale transfer of kinetic energy via the triadic interactions. The slightly negative mean transfer at $n = 2$ ($\kappa_n \ell_k = 0.782$) is attributed to numerical artifacts associated with computing discrete wavelet coefficients, rather than upscale energy transfer (or backscatter) on average. The maximum SFS transfer for all three cases occurs at $\kappa \ell_k \approx 0.2$, within the inertial subranges shown in Fig. 5(a). The maximum Π_{SFS} decreases monotonically as $\mathrm{St}_{k,0}$ increases, consistent to the description of Ferrante and Elghobashi [19] about the triadic interactions.

For no-particle and $\mathrm{St}_{k,0} = 10$ cases, the downscale transfer is negligibly small at $\kappa \ell_k \gtrsim 0.8$, leaving only the viscous mechanisms in changing TKE [for $\mathrm{St}_{k,0} = 10$, mean $\check{T}_\psi$ is nearly zero, as shown in Fig. 5(b)]. On the other hand, the mean downscale transfer remains finite at $\kappa \ell_k \gtrsim 0.8$ for the critical particles. This suggests that the wave-number range in which the triadic interactions prevail is extended on average toward small scales by the interphase interactions involving $\mathrm{St}_{k,0} = 1$ particles. Regardless of the Stokes number, all decaying HITs in this study exhibit scale locality in energy transfer [28] (not shown), estimated using Eq. (23). Thus, the enhanced downscale transfer of kinetic energy is associated with draining more energy from larger scales. Then, increased small-scale TKE shown in Fig. 5(a) for $\mathrm{St}_{k,0} = 1$ is a combined consequence of the critical point particles invigorating small-scale turbulent eddies [Fig. 5(b)] and strengthening the energy cascade. A similar

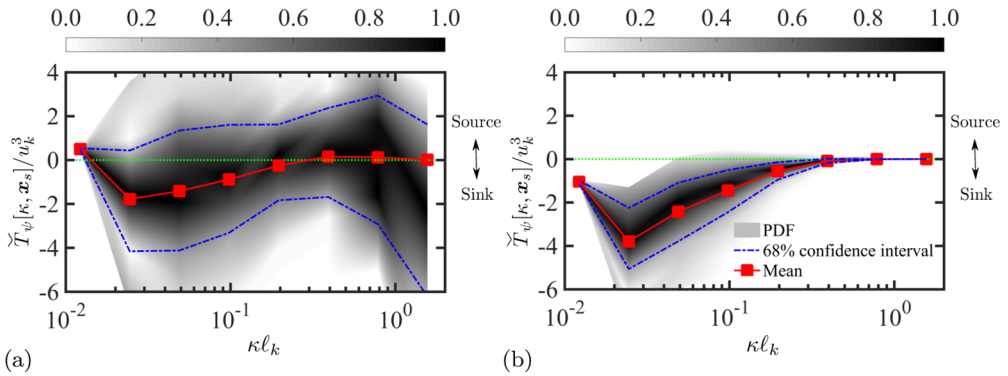

FIG. 7. Contours of scale-dependent PDF of energy transfer due to the particle drag at $\Delta t/t_\ell = 0.64$ for (a) $\mathrm{St}_{k,0} = 1$ and (b) $\mathrm{St}_{k,0} = 10$. The horizontal dotted lines denote the neutral interphase transfer.

argument is made by Ferrante and Elghobashi [19], but their interscale flux $T[\kappa]$ measures only a net change of flux at a scale without explicitly considering the cross-scale transfer. As discussed in regard to Eq. (22), $T[\kappa]$ is not exempt only from interactions between superfilter scales [28]. Thus, $T[\kappa]$ alone does not inform explicitly the direction (in the spectral space) of energy transfer, unlike Π_{SFS} [28] does.

C. Local wavelet statistics

Mean wavelet statistics presented in Sec. IV B show turbulence modulation consistent with the Fourier analysis of decaying HIT suspended with point particles. However, their spatial variations are stripped off (the same as the Fourier analysis) since the scale-dependent average $\langle\,\rangle_{\boldsymbol{x}_s}$ is taken. When inertial particles are accumulated preferentially in space, as illustrated in Fig. 1(a), such averaging artifacts are not insignificant. For instance, $\Pi_{\mathrm{SFS}}[\kappa] \approx 0$ in Fig. 6 indicates in-scale transfer on average at wave number κ. However, this does not necessarily mean that clustered particles do not contribute to cross-scale energy transfer at every location in space (at that scale). As will be shown later, such clusters are often associated with strong local cross-scale transfer of kinetic energy, but upscale and downscale transfers nearly cancel out when averaged in space. Similar observations are made for the interphase energy transfer. For instance, $\check{T}_\psi > 0$ [in Fig. 5(b)] does not mean that particles behave as local energy sources everywhere at that scale. Detailed information on spatial locality of turbulence and particle statistics is useful for SGS modeling. With interphase and interscale energy transfer available as a function of scale and position, *a priori* estimation of SGS stress can be improved in two-way coupled setups. Also, correlation between local particle concentration and SGS stress can be developed. In this section, local wavelet statistics are examined by retaining spatial variabilities of wavelet energy spectra and fluxes [31,33,38].

Figure 7 shows the contours of a normalized probability density function (PDF) of energy transfer due to the particle drag force at $\Delta t/t_\ell = 0.64$. At each scale, the maximum PDF is normalized to unity before constructing the contours. The solid line with symbols corresponds to the scale-dependent mean transfer $\check{T}_\psi[\kappa]$ [the same as those in Fig. 5(b)], and the gray-scale contours show the spatial variabilities of $\check{T}_\psi[\kappa, \boldsymbol{x}_s]$, quantified by the 68% confidence intervals. Compared with Fig. 5(b), Stokes-number dependence is more evident across all scales. For $\mathrm{St}_{k,0} = 1$ [Fig. 7(a)], the spatial variabilities of the interphase transfer $\check{T}_\psi$ are considerably higher than those of $\mathrm{St}_{k,0} = 10$ [Fig. 7(b)]. This is expected as the critical particles accumulate inhomogeneously at high concentration and thus the velocity slip varies significantly in space. This implies that certain correlations may exist between local particle concentration and spectral energy transfer, as $\check{T}_\psi$ triggers turbulence modulation in the carrier phase [19,40]. Such correlations can be useful to develop supplementary SGS models incorporating the two-way coupling effects in LES closure.

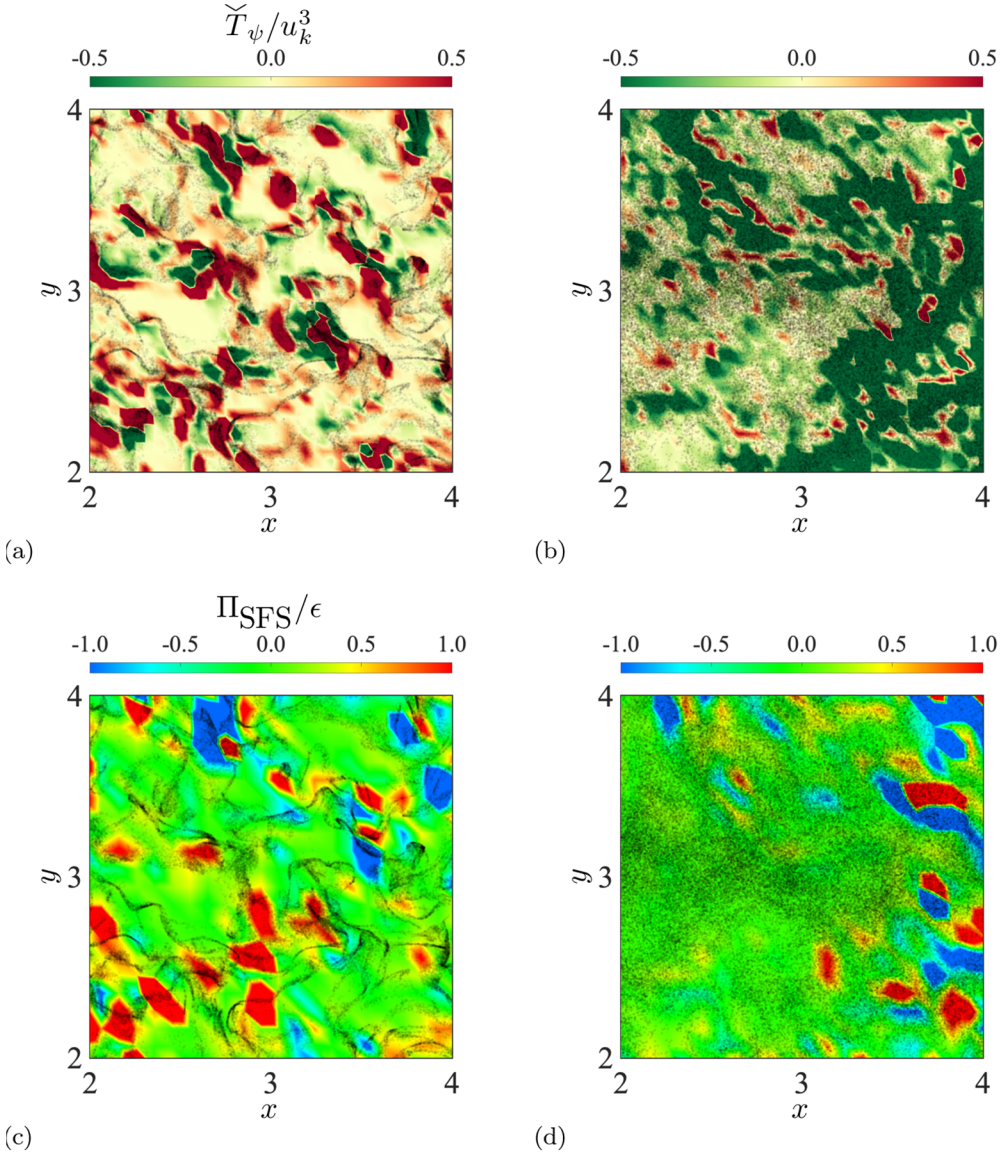

FIG. 8. Instantaneous contours of energy transfer due to the particle drag force at $s = 1$ for (a) $\mathrm{St}_{k,0} = 1$ and (b) $\mathrm{St}_{k,0} = 10$. The SFS energy transfer due to the triadic interactions at $s = 2$ for (c) $\mathrm{St}_{k,0} = 1$ and (d) $\mathrm{St}_{k,0} = 10$. All figures are obtained on a part of the x-y midplane and at $\Delta t/t_\ell = 0.64$. The contours are overlaid with particles.

Also, Fig. 7(a) shows that the clusters of $\mathrm{St}_{k,0} = 1$ particles are not definite energy sources or sinks locally in space, although on average they are sources at small scales and sinks at large scales (similar to what Fourier analysis shows). This is the case not only statistically [Fig. 7(a)] but also instantaneously [Fig. 8(a)], where local interphase fluxes at $s = 1$ closely correlated with clustered $\mathrm{St}_{k,0} = 1$ particles do not take the same sign. As expected, $\breve{T}_\psi$ takes near-zero values where particles are scarce. Such spatially local details of statistics are not available in the Fourier analysis as its spatial dependence is completely removed in evaluating the discrete Fourier transform. In contrast to $\mathrm{St}_{k,0} = 1$, heavy particles ($\mathrm{St}_{k,0} = 10$) remain as consistent energy sinks at every scale

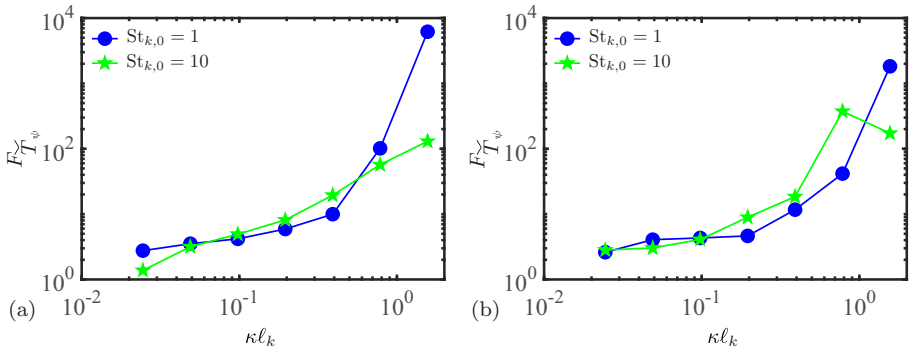

FIG. 9. Flatness of the interphase coupling term at (a) $\Delta t/t_\ell = 0.16$ and (b) $\Delta t/t_\ell = 0.64$. Flatness factors at the largest scale ($s = 8$) are not shown.

and position, as shown in Fig. 7(b). A similar observation is made for the contours at other time instants.

Figure 9 shows the flatness factor of the interphase coupling term $\check{T}_\psi$ at $\Delta t/t_\ell = 0.16$ and 0.64. For $\mathrm{St}_{k,0} = 1$, strong intermittency is observed at the smallest scale where particles and Kolmogorov eddies interact most significantly, as measured by the flatness being an order of magnitude higher than that of $\mathrm{St}_{k,0} = 10$. Bassenne *et al.* [33] reported the flatness of wavelet spectra of particle concentration several orders higher for $\mathrm{St}_k = 1$ than 10, also confirmed by the current study (not shown). Since the flow is not externally forced, turbulent fluctuations become weaker in time. Thus, the same particles behave more tracerlike, and the degree of the preferential concentration is reduced, which is manifested by lower flatness values at the smallest scale for $\mathrm{St}_{k,0} = 1$ in Fig. 9(b).

Contour plots similar to Fig. 7 are shown for the SFS energy flux in Fig. 10 at $\Delta t/t_\ell = 0.64$. The solid lines (mean transfer) are plotted for reference and correspond to those in Fig. 6(b). For $\mathrm{St}_{k,0} = 1$ [Fig. 10(b)], the spatial variabilities of the SFS energy flux are enhanced significantly at small scales (for downscale energy transfer, in particular) compared with unladen HIT [Fig. 10(a)]. Considering that qualitative features of the carrier phase with and without the critical particles are similar where particles are scarce [19], a question arises as to whether the enhanced cross-scale transfer is associated with the spatially localized clusters of the critical particles or more nonlocal in space. However, Fig. 10(b) alone does not provide such information, since, unlike

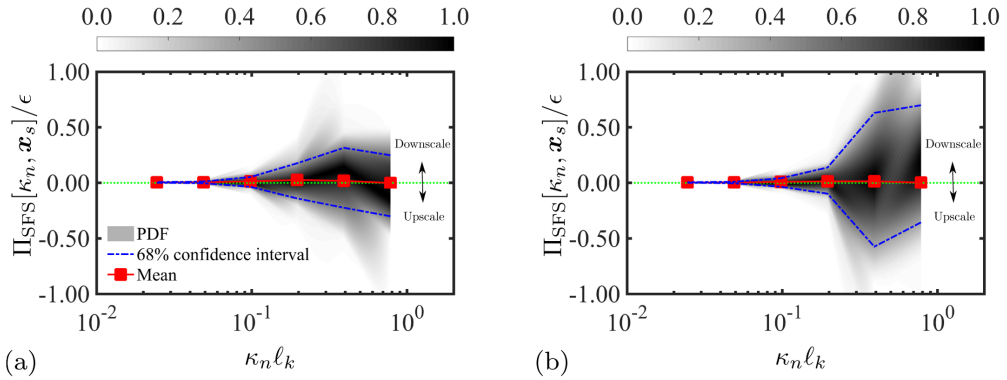

FIG. 10. Scale-dependent PDF of the cumulative detailed energy fluxes due to the convective and pressure transports for (a) no-particle and (b) $\mathrm{St}_{k,0} = 1$ at $\Delta t/t_\ell = 0.64$. Cutoff scale n is shown for $n = 2$ through 7. The horizontal dotted lines denote the in-scale transfer.

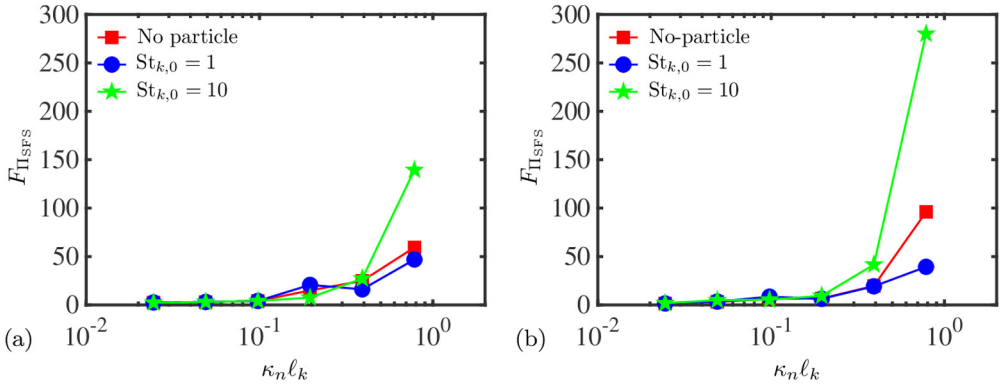

FIG. 11. Flatness of the cumulative detailed SFS energy fluxes at (a) $\Delta t/t_\ell = 0.16$ and (b) $\Delta t/t_\ell = 0.64$. Cutoff scale n is shown for $n = 2$–7.

$\check{T}_\psi$, the SFS energy flux is calculated regardless of the presence of particles (that is, Π_{SFS} is a carrier-phase quantity). The above question is addressed in Sec. V, where wavelet statistics are conditioned on particle concentration so that interphase and interscale information can be analyzed simultaneously.

The flatness of the SFS energy flux due to the triadic interactions is shown in Fig. 11. The SFS transfer becomes increasingly intermittent toward small scales for all three cases. However, the cutoff scale $n = 2$ shows a distinct Stokes-number dependence. Intermittency of Π_{SFS} is lower at small scales for $\mathrm{St}_{k,0} = 1$ than the single-phase turbulence and $\mathrm{St}_{k,0} = 10$. This trend is opposite to the interphase transfer $\check{T}_\psi$ shown in Fig. 9, where $\mathrm{St}_{k,0} = 1$ is associated with the largest degree of intermittency. Reduced intermittency of Π_{SFS} for $\mathrm{St}_{k,0} = 1$ implies that such particles clustered locally in space are not associated with particularly strong local downscale or upscale transfer of TKE, and cross-scale transfer is enhanced presumably in a way more nonlocal in space. This will be discussed further in the next section.

V. CONDITIONED WAVELET STATISTICS

To better describe the interphase cross-scale interactions, conditioned statistics are examined. Initial attempts were made by conditioning based on a quantity defined on the primitive DNS grid, similar to Kim *et al.* [31]. This is motivated by an observation that the preferential concentration occurs locally in space and thus the maximum spatial resolution is desired for conditioning. However, little or no sensitivity is observed when statistics are conditioned using particle-number density, enstrophy, or volume fraction defined on the DNS grid.

Alternatively, wavelet statistics are conditioned based on particle-number density coarse grained on the wavelet colocation grid. Coarse graining is a useful tool to reveal a multiscale nature of turbulence (see, for example, Aluie [42]). Bassenne *et al.* [33] analyzed forced HIT laden with one-way coupled point particles using the same conditioning method. For some of the results shown in this section, the Haar wavelet is also used, as it offers the highest degree of spatial localization and consistency with coarse graining. Although the Haar basis suffers from spectral leakage, the average wavelet statistics computed using the Haar and Coifman (used in Sec. IV) wavelets are qualitatively similar, and trends are consistent with each other, as demonstrated in Figs. 12(a) and 12(b) for Π_{SFS} and $\check{T}_\psi$, respectively.

A. Joint wavelet statistics for $\mathrm{St}_{k,0} = 1$

For $\mathrm{St}_{k,0} = 1$, Fig. 13 shows the joint PDF of fluctuation of the logarithm of the local wavelet energy spectrum, $(\ln\check{E})' = \ln\check{E} - \langle\ln\check{E}\rangle_{\boldsymbol{x}_s}$, and coarse-grained number density. The former variable

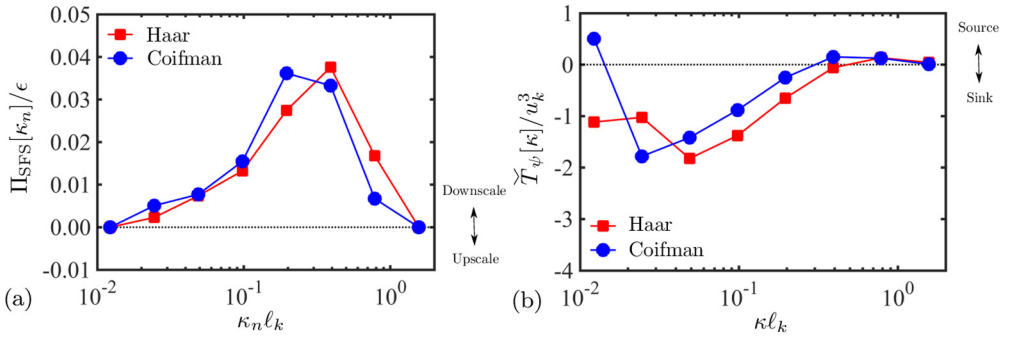

FIG. 12. Comparisons of (a) the mean detailed cumulative energy fluxes due to the triadic interactions, and (b) the mean spectral energy transfer due to the particle drag force, computed using the Haar and 24-point Coifman bases. Both plots are obtained for $\mathrm{St}_{k,0} = 1$ and at $\Delta t/t_\ell = 0.16$. The horizontal dotted lines denote (a) the in-scale and (b) the neutral interphase transfers, respectively.

represents a deviation from the mean wavelet spectral energy at a given scale and position [33]. The horizontal and vertical axis variables are normalized by the standard deviation and the global mean number density $\langle n \rangle = n_0$, respectively. The conditional mean of coarse-grained number density is shown as a solid line. Only the first three scales ($s = 1$–3) are shown at $\Delta t/t_\ell = 0$ (first column) and 0.16 (second column).

At $\Delta t/t_\ell = 0$, the interphase coupling Eq. (3) is activated, and both phases still behave similarly to those of one-way coupled HIT examined by, for instance, Bassenne *et al.* [33] (see Figs. 8 and 10 in their article). Conditional-mean concentration and fluctuating spectral energy are anticorrelated at small scales, showing that particles exist at concentration higher than the mean number density where turbulent motions are weak, consistent with the preferential concentration [1]. The carrier phase is characterized by a large volume of regions devoid of particles, indicated by the maximum PDF near the origin ($s = 1$, in particular). At larger scales, the PDF peak gradually approaches $\langle n \rangle = n_0$, as the preferential concentration is a small-scal e phenomenon.

At $\Delta t/t_\ell = 0.16$ ($3.4t_k$ after the two-way coupling is activated), the joint PDF shows distinct qualitative differences. Since the forcing is turned off at $\Delta t/t_\ell = 0$ and turbulence begins to decay, statistics are time-dependent. Thus, comparing statistics between $\Delta t/t_\ell = 0$ and 0.16 should be done with care, as the instantaneous Stokes number becomes lower than unity. However, TKE at $\Delta t/t_\ell = 0.16$ decreases by 14% [see Fig. 2(a)], which lies within the range of TKE fluctuation for the constant-ϵ forcing that this study uses for one-way coupled simulation [see Fig. 1(a) of Bassenne *et al.* [36]]. Also, the dissipation rate remains nearly the same ($\lesssim 3.8\%$) during the initial $0.16t_\ell$, as shown in Fig. 2(b). Thus, the Stokes number at $\Delta t/t_\ell = 0.16$ is 0.98 as Fig. 3 shows, justifying a comparison between $\Delta t/t_\ell = 0$ and 0.16.

At $\Delta t/t_\ell = 0.16$, the joint PDF contours remain qualitatively similar to those at $\Delta t/t_\ell = 0$, showing that particles are still accumulated preferentially in space. However, unlike the one-way coupled case (see, for example, Bassenne *et al.* [33]), the conditional mean is not anticorrelated with fluctuating energy where TKE is stronger than the average, namely where $(\ln \check{E})' > 0$ ($s = 1$ and 2, in particular). In other words, clusters of highly concentrated two-way coupled $\mathrm{St}_{k,0} = 1$ particles are found where turbulent motions are stronger than the average. This is associated with Fig. 5(a), where the small-scale mean spectral energy is amplified for $\mathrm{St}_{k,0} = 1$. With Fig. 5(b), it follows that the clustered critical particles modulate the carrier-phase turbulence in such a way that local fluid velocity at small scales is aligned, on average, with the Stokes drag force and thus local TKE is enhanced. However, as shown in Fig. 7(a) (and later confirmed in Fig. 14), such particle

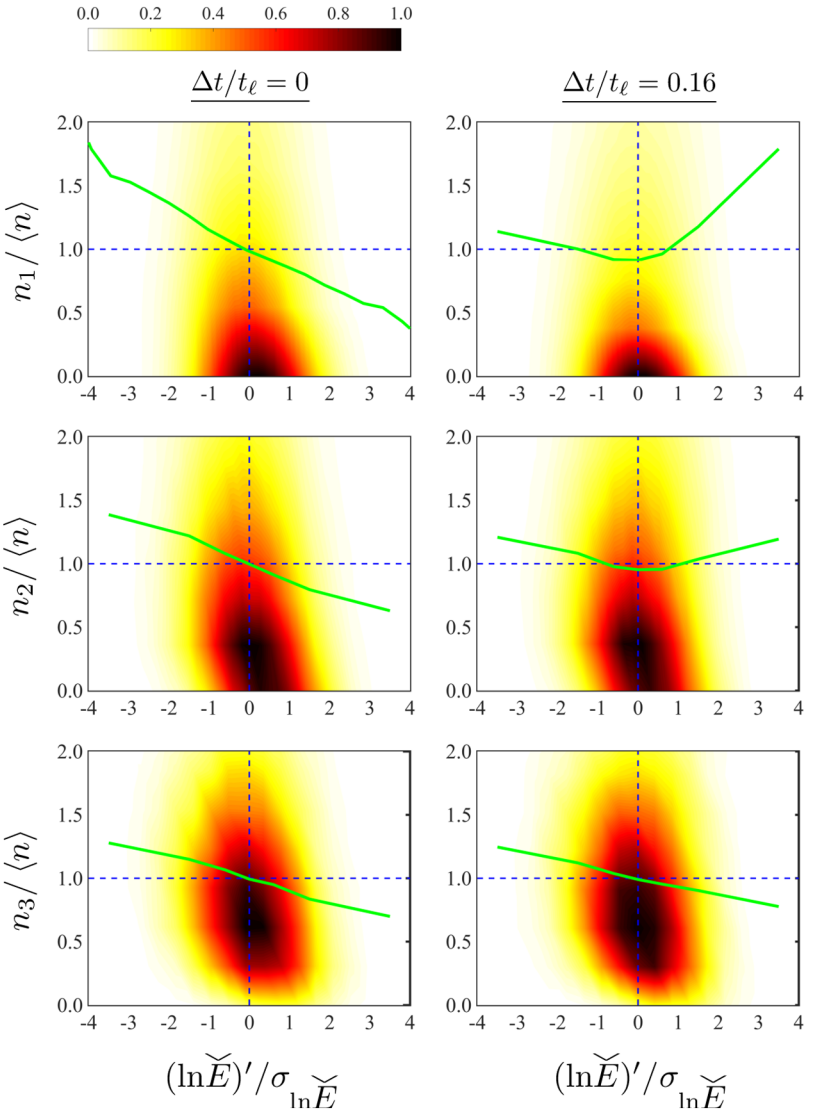

FIG. 13. Joint PDF of coarse-grained particle-number density and fluctuation of the logarithm of the local wavelet spectrum of kinetic energy for $\mathrm{St}_{k,0} = 1$. The first three scales are shown at $\Delta t/t_\ell = 0$ (first column) and 0.16 (second column). The solid line denotes the conditional mean of coarse-grained particle-number density.

clusters are not definite local energy sources. At larger scales ($s = 3$), the two-way coupling effects diminish, and the joint PDF remains the same as the one-way coupled case.

In Fig. 14, a joint PDF of coarse-grained particle-number density and interphase energy transfer is shown at $\Delta t/t_\ell = 0.16$ for $\mathrm{St}_{k,0} = 1$. The void zones discussed in Fig. 13 are correlated with near-zero $\breve{T}_\psi$ (neither source nor sink), which is consistent with Fig. 8(a). At $s = 1$–3, the conditional mean is nearly symmetric with respect to $\breve{T}_\psi = 0$, showing that there is no average preference for highly concentrated $\mathrm{St}_{k,0} = 1$ particles behaving as a definite source or sink of TKE. From LES modeling perspectives, the above observations suggest that the resolved interphase energy transfer cannot be deemed a source of resolved TKE from the dispersed phase

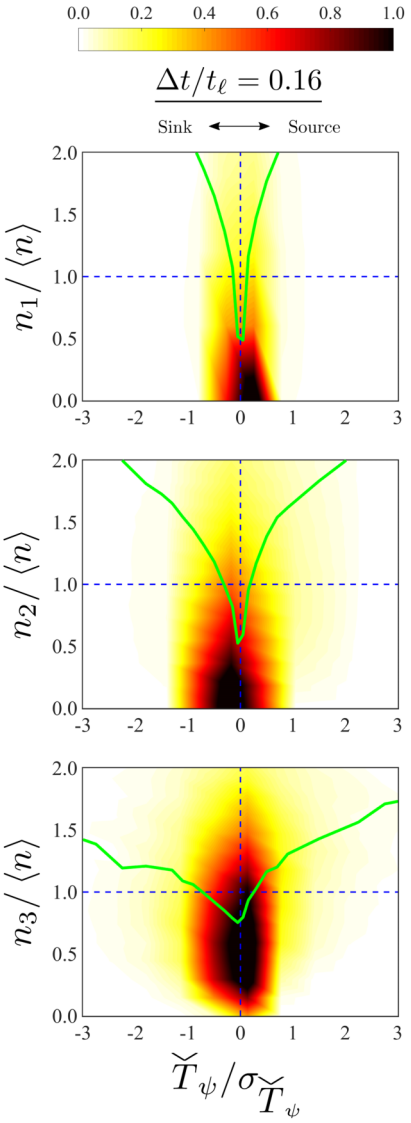

FIG. 14. Joint PDF of coarse-grained particle-number density and energy transfer due to the particle drag force for $\mathrm{St}_{k,0} = 1$. The first three scales are shown at $\Delta t/t_\ell = 0.16$. The solid line denotes the conditional mean of coarse-grained particle-number density.

(as the Fourier analysis suggests) and should be modeled to have, for instance, a bimodal-like distribution.

A joint PDF of the SFS energy flux due to the triadic interactions and coarse-grained particle-number density is shown for $\mathrm{St}_{k,0} = 1$ in Fig. 15. At $s = 2$ (the first row), regions devoid of particles are characterized distinctly by the in-scale transfer ($\Pi_{\mathrm{SFS}} \approx 0$). However, the inverse is not true in general; the in-scale transfer does not necessarily indicate negligible particle concentration [also illustrated in Fig. 8(b)]. At $\Delta t/t_\ell = 0$ (first column), particle concentration is anticorrelated weakly with the amplitude of the cross-scale energy flux. This is expected since one-way coupled particles tend to avoid regions of strongly turbulent motions, and the interphase coupling is just activated. At $\Delta t/t_\ell = 0.16$ (second column) when particles are allowed to affect turbulence, such a trend

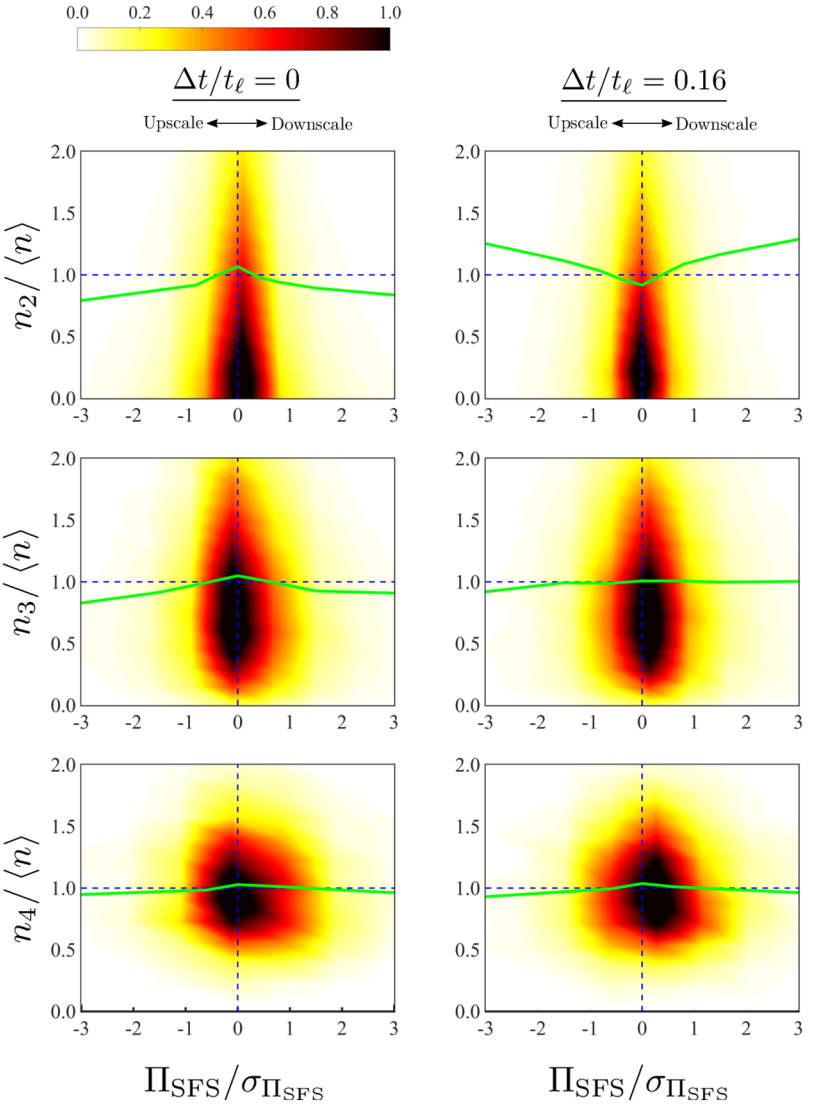

FIG. 15. Joint PDF of coarse-grained particle-number density and the cumulative SFS energy flux for $\mathrm{St}_{k,0} = 1$. Scales $s = 2$ (top row), 3 (middle row), and 4 (bottom row) are shown at $\Delta t/t_\ell = 0$ (first column) and 0.16 (second column). The solid line denotes the conditional mean of coarse-grained particle-number density.

is reversed and high-particle concentration is associated with stronger (in magnitude) cross-scale energy transfer. Similar to $\check{T}_\psi$, clusters of $\mathrm{St}_{k,0} = 1$ particles do not have a preference on average down- or upscale SFS transfer as the symmetric (with respect to $\Pi_{\mathrm{SFS}} = 0$) conditional mean shows. Such two-way coupling effects are restricted at the smallest scale, and particle concentration becomes insensitive to Π_{SFS} at larger scales. Also, the joint PDF becomes close to that of the random distribution (see $s = 4$, for instance).

Figure 16 shows the joint PDF of interphase and cross-scale fluxes for $\mathrm{St}_{k,0} = 1$. Since both Π_{SFS} and $\check{T}_\psi$ do not involve coarse graining, the 24-point Coifman wavelet is used to reduce spectral leakage. Although the average wavelet statistics are insensitive to the choice of basis, as shown in Fig. 12, spectral leakage is still present when the Haar wavelet is used. With the Coifman basis, the effects of spectral leakage on joint PDF and observations made regarding Figs. 13–15 can

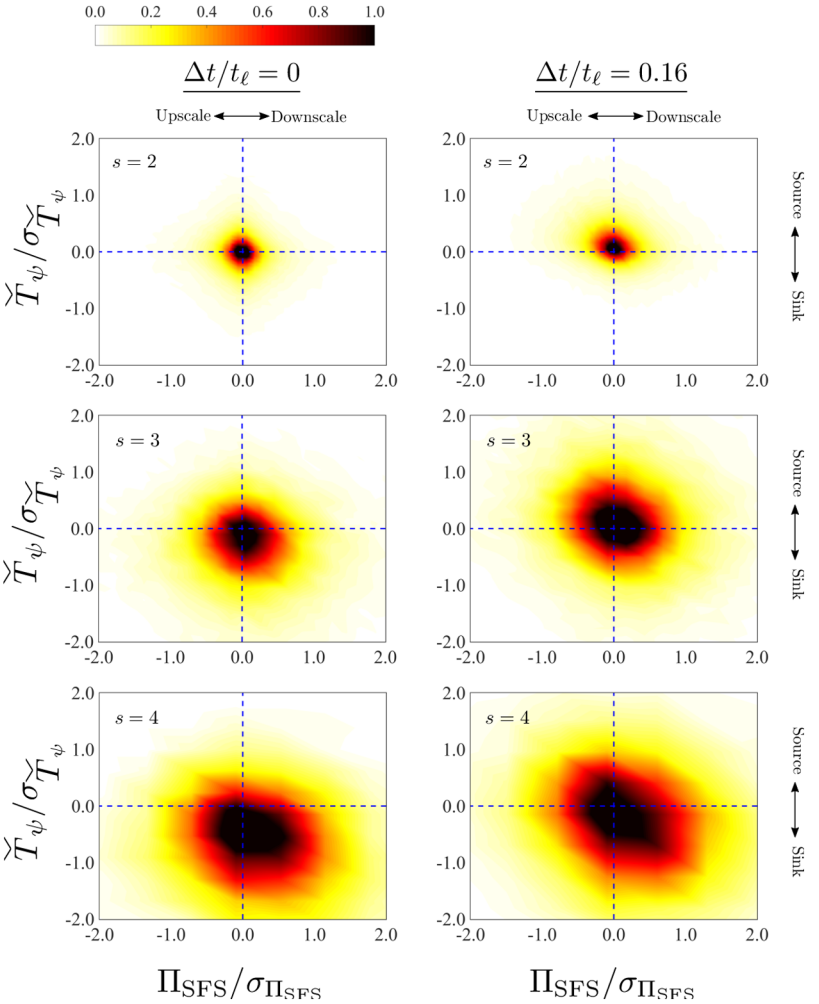

FIG. 16. Joint PDF of energy transfer due to the particle drag force and the cumulative SFS energy flux for $\mathrm{St}_{k,0} = 1$. Scales $s = 2$ (top row), 3 (middle row), and 4 (bottom row) are shown at $\Delta t/t_\ell = 0$ and 0.16. Wavelet statistics are computed using the 24-point Coifman wavelet basis.

be reduced. In Fig. 16, each subfigure is characterized by four quadrants. For instance, the first quadrant is associated with the downscale transfer (forward-scatter) of kinetic energy by the triadic interactions and the interphase coupling that amplifies kinetic energy at each scale and location. Compared with $\Delta t/t_\ell = 0$ when the coupling force Eq. (3) is just activated, the two-way coupling effects at $\Delta t/t_\ell = 0.16$ are manifested by substantial interphase energy from dispersed to carrier phases (first two quadrants). Such energy transfer is correlated with both upscale and downscale transfer, consistent with observations made regarding Figs. 10 and 15. At larger scales, particles attenuate TKE where its downscale transfer prevails, which is, however, markedly different from $\Delta t/t_\ell = 0$ in that particles also behave as strong energy sources. Overall, joint PDF evaluated using the Coifman basis results in observations that are qualitatively consistent with those using the Haar basis.

B. Joint wavelet statistics for $\mathrm{St}_{k,0} = 10$

The WMRA framework can be applied to analyze the interphase, cross-scale transfer of turbulent flows laden with $\mathrm{St}_{k,0} = 10$ particles. Compared with the $\mathrm{St}_{k,0} = 1$ case, TKE and dissipation rate decay much more rapidly due to the high inertia of particles (see Fig. 2). Thus, it is not useful to directly compare two different snapshots as they are in drastically different conditions. For instance, Fig. 3 shows that the Stokes number estimated at $\Delta t/t_\ell = 0.64$ for $\mathrm{St}_{k,0} = 10$ is only 40% of the initial Stokes number. In this section, only wavelet statistics at $\Delta t/t_\ell = 0.64$ are shown to demonstrate that WMRA describes consistently the two-way interactions between heavy particles and HIT. However, joint wavelet statistics are similar at different time instants due to relatively high Stokes numbers ($\mathrm{St}_k > 4$).

In Fig. 17, the first column shows the joint PDF of particle-number density and wavelet spectral energy for $\mathrm{St}_{k,0} = 10$. The PDF peaks are located at $n_s/\langle n\rangle \approx 0.8$ at all scales, showing no sign of preferential concentration (as expected). In one-way coupled simulation (not shown), the contours are symmetric with respect to $(\ln \check{E})' = 0$, and the conditional mean is nearly constant as $\langle n\rangle$ regardless of fluctuating spectral energy. When the two-way coupling is activated, the conditional mean becomes a strong function of $(\ln \check{E})'$, rendering heavy particles more sensitive to local flow conditions and less ballistic. The second column shows the joint PDF of particle-number density and the interphase energy transfer. Unlike $\mathrm{St}_{k,0} = 1$ in Fig. 14, clear asymmetry of the contours with respect to $\check{T}_\psi = 0$ is found since heavy particles act primarily as local energy sinks, as shown in Fig. 7(b). The SFS energy transfer is shown in the third column. Since Π_{SFS} is identically zero at the cutoff scale $n = 1$, only $n = 2$ and 3 are shown. Unlike $\mathrm{St}_{k,0} = 1$ where particle-number density and the SFS energy flux are decorrelated at $n \gtrsim 3$ and the contours become similar to those of a random distribution (see the second column of Fig. 15), cross-scale energy transfer remains correlated with a local concentration of point heavy particles. Such observations are useful to understand the effects of two-way coupled inertial particles on SGS modeling of turbulent flows, as discussed in the next section.

C. *A priori* interpretation for the SGS modeling of two-way coupled particle-laden turbulence

Some of the findings in this study provide useful insight for a LES modeling of turbulence suspended with point inertial particles coupled in two ways with the carrier phase. In particular, scale-dependent joint wavelet statistics evaluated locally in space are useful for characterizing the interactions of SFS motions with larger, resolved scales in the presence of inertial particles. In particular, $\mathrm{St}_{\mathrm{SGS}}$ [17] is used to describe the two-way coupling effects on the particle and carrier phase. In the limit of $\mathrm{St}_{\mathrm{SGS}} \ll 1$, the effects of SGS motions on particle aerodynamics are significant (SGS-noninertial), requiring additional models that take into account such effects in Eq. (5) as examined recently by Park *et al.* [43] and previously by many others for one-way coupled setups. However, SGS-noninertial particles relax quickly to the motions of eddies larger than ℓ_Δ, and thus even if the mass loading ratio is of the order of unity, their direct impacts on the resolved scales of turbulence remain insignificant (SGS loaded) [17]. For $\mathrm{St}_{\mathrm{SGS}} \gg 1$, interphase interactions show the opposite trends. High-inertia particles are ballistic in nature and slip primarily with respect to resolved eddies. Such particles are SGS inertial, and the subgrid contributions to Eq. (5) are less pronounced than SGS-noninertial particles. On the other hand, the carrier phase becomes SGS unloaded, and its resolved scales interact strongly with $\mathrm{St}_{\mathrm{SGS}} \gg 1$ particles if $\alpha = O(1)$ [17].

Conditioned wavelet statistics discussed in Secs. V A and V B show such limiting behaviors in an *a priori* sense. The LES filter width is associated with the scale-dependent wavelet grid spacing, $\ell_\Delta \sim \ell_s = 2^s\Delta$. Following Urzay *et al.* [17], $\mathrm{St}_{\mathrm{SGS}} \sim \mathrm{St}_k(\ell_k/\ell_\Delta)^{2/3}$, which makes the scale-dependent $\mathrm{St}_{\mathrm{SGS}}$ smaller than St_k [43]. As a result, joint PDF contours of number density and TKE fluctuations shown in Fig. 13 for $\mathrm{St}_{k,0} = 1$ show SGS-loaded characteristics ($\mathrm{St}_{\mathrm{SGS}} \ll 1$), in particular, at large scales. For instance, at $s = 3$ (third row), both the joint PDF and the conditional mean remain similar before and after the two-way coupling becomes effective on average at $\Delta t/t_\ell \approx 0.16$ [or $\Delta t/t_k \approx 3.3$; see Fig. 4(a)]. In the LES context (*a priori*), this shows that the

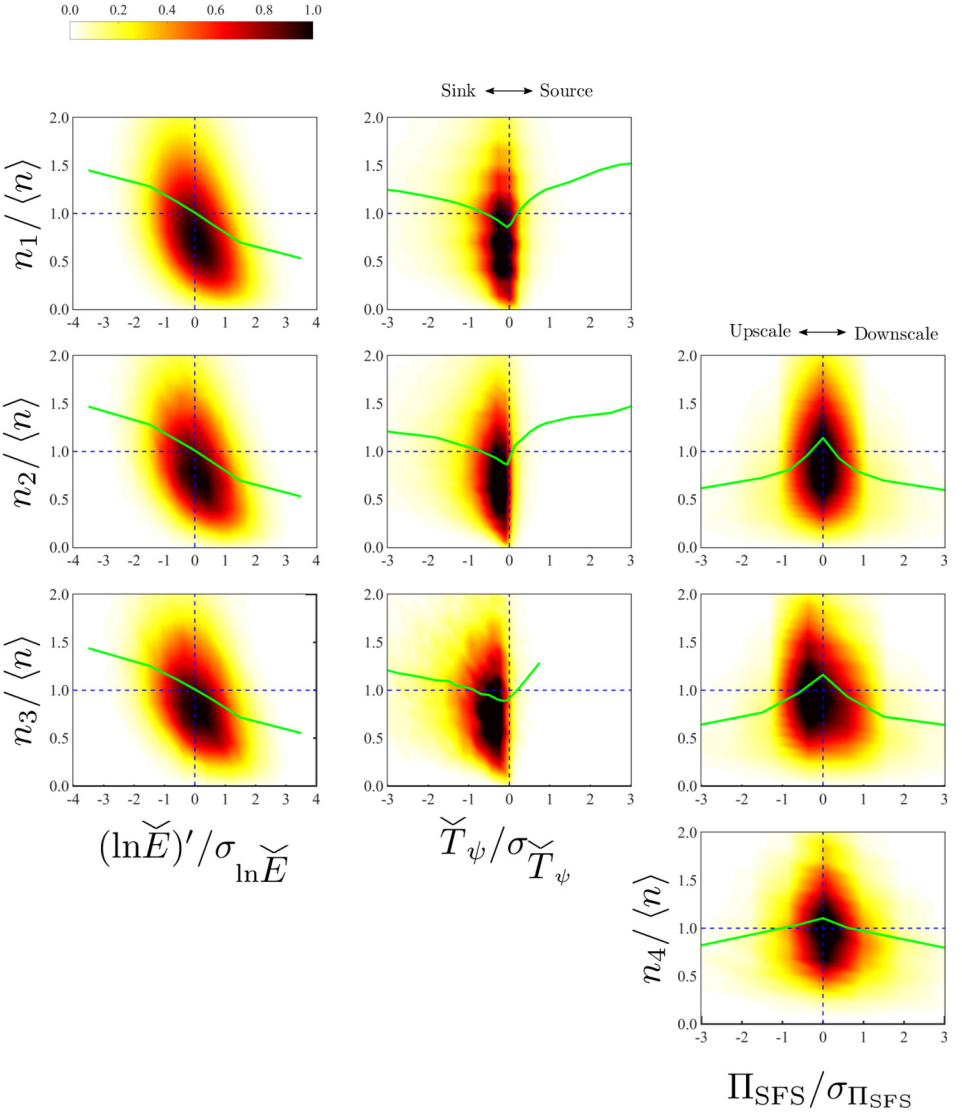

FIG. 17. Joint PDFs of coarse-grained particle-number density and (a) fluctuation of the logarithm of the local wavelet spectrum of kinetic energy (first column), (b) energy transfer due to the particle drag force (second column), and (c) the cumulative SFS energy flux (third column). For $\mathrm{St}_{k,0} = 10$, the first three scales are shown at $\Delta t/t_\ell = 0.64$. The solid line denotes the conditional mean of coarse-grained particle-number density.

interphase interactions involving the two-way coupled $\mathrm{St}_{k,0} = 1$ particles occur in such a way that resolved scales of $O(\ell_3 \approx 16\ell_k)$ (and also for $s > 3$ not shown here) are not modulated significantly by $\mathrm{St}_{\mathrm{SGS}} \ll 1$ particles, consistent with the scaling argument of Urzay *et al.* [17] for the SGS-loaded case. However, this is not the case for smaller scales ($s = 1$ and 2) where conditional mean is altered significantly. This is presumably due to $\mathrm{St}_{\mathrm{SGS}}$ less than unity but not vanishingly small so that $\mathrm{St}_{\mathrm{SGS}} \ll 1$ is met.

On the other hand, the SGS-unloaded behavior is found for $\mathrm{St}_{k,0} = 10$, as shown in the first column of Fig. 17. Indeed, HIT laden with heavy particles decays quickly so that the instantaneous Stokes number is less than $\mathrm{St}_{k,0} = 10$. However, $\mathrm{St}_k \approx 4$ at $\Delta t/t_\ell = 0.64$ is still greater than unity (as shown in Fig. 3), and wavelet statistics at earlier times are qualitatively similar. For all scales

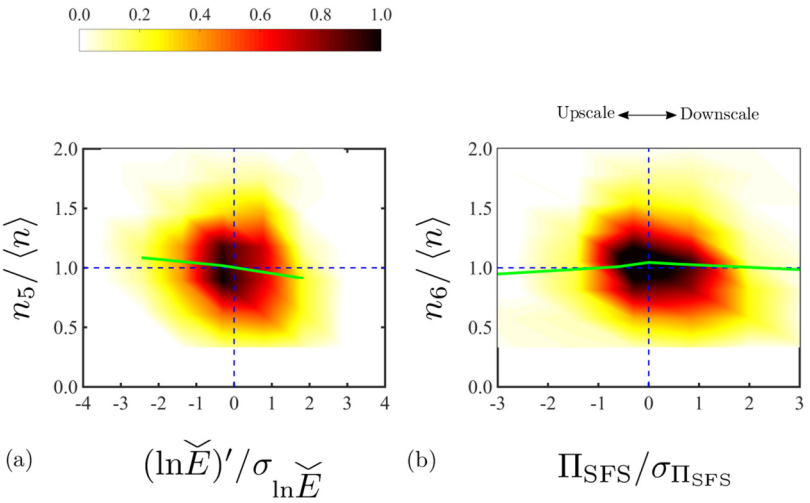

FIG. 18. Joint PDFs of coarse-grained particle-number density and (a) fluctuation of the logarithm of the local wavelet spectrum of kinetic energy and (b) the SFS energy flux. The joint statistics are obtained for $\mathrm{St}_{k,0} = 10$ at $\Delta t/t_\ell = 0.64$. The solid line denotes the conditional mean of coarse-grained particle-number density.

shown in Fig. 17, the two-way coupling takes effects in a similar way. Joint PDF contours are tilted (compared with those of the corresponding one-way coupled simulation not shown here), and conditional mean number density becomes a stronger function of TKE fluctuations. Thus, $\mathrm{St}_k = 4$ particles slip with respect to all scales shown in Fig. 17 (and larger scales as well), which demonstrates, in an *a priori* sense, effective modulations of resolved scales by point heavy particles. Estimated $\mathrm{St}_{\mathrm{SGS}}$ is approximately greater than unity for $s = 1$–3 (thus, SGS unloaded, at least weakly), consistent with the scaling argument [17]. At larger scales ($s \gtrsim 5$), $\mathrm{St}_{\mathrm{SGS}}$ becomes smaller than unity, thus rendering heavy particles nonballistic with respect to $\ell_\Delta \gtrsim \ell_5 \approx 63\ell_k$. As a result, joint PDF contours [shown in Fig. 18(a)] become similar to those of $\mathrm{St}_{k,0} = 1$ at large scales (see, for instance, the third row of Fig. 13), and turbulence modulation at $s \gtrsim 5$ by $\mathrm{St}_{k,0} = 10$ particles is insignificant [see Fig. 18(b)].

The above observations involving $\mathrm{St}_{k,0} = 1$ and 10 particles suggest a useful clue for designing a LES study of two-way coupled particle-laden turbulence in terms of SGS modeling and LES grid resolution. For instance, $\mathrm{St}_{k,0} = 1$ particles induce reduced modulations of large-scale motions of turbulence. In an *a priori* sense, this implies that existing SGS models designed for single-phase turbulence can be applied if the SGS loaded behavior is preserved by choosing a moderate-sized LES grid spacing. However, if the LES grid is refined (say, $\Delta \lesssim 4\ell_k$, in this particular case), resolved fluid motions are not SGS loaded anymore, and the SGS closure should consider interphase transfer. For $\mathrm{St}_{k,0} = 10$, interphase contributions to SGS closure seem essential regardless of LES grid resolution, as Fig. 17 supports in an *a priori* sense. This suggests the need to develop a new SGS model that takes into account such effects. It is noted, however, that interphase contributions to the SGS model should vanish as LES grid resolution becomes coarse (say, $\Delta \gtrsim 63\ell_k$, in this particular case) since $\mathrm{St}_{\mathrm{SGS}}$ becomes lower than unity.

Similar observations are made for cross-scale energy transfer estimated by the SFS energy flux Π_{SFS}. For $\mathrm{St}_{k,0} = 1$, the SFS energy transfer becomes largely decorrelated with particle concentration at $s \gtrsim 3$, as the conditional mean shows in Fig. 15 (second column). Also, joint PDF resembles that of the randomly distributed particles [33] with its peak slightly shifted toward the downscale transfer. In addition, there is little qualitative difference before and after the two-way coupling is activated. However, strong correlation between the magnitude of Π_{SFS} and coarse-grained number density is found for $s = 2$. These observations suggest that for a typical choice of LES filter size

(that is, $\ell_\Delta \gg \ell_k$), the carrier phase laden with point $\mathrm{St}_k = 1$ particles is SGS loaded ($\mathrm{St}_{\mathrm{SGS}} \ll 1$), and modulation of resolved-scale turbulence quantified by Π_{SFS} is not significant. For $\mathrm{St}_{k,0} = 10$ (or $\mathrm{St}_k = 4$ at $\Delta t/t_\ell = 0.64$), however, both the joint PDF and the conditional mean are modified consistently, as shown in the third column of Fig. 17. This shows direct evidence of point heavy particles modifying the SFS energy transfer of the carrier-phase turbulence (qualitatively similar joint wavelet statistics are obtained at earlier times when the instantaneous Stokes numbers are higher than 4). Figure 17 also shows that the two-way coupling effects of heavy particles on turbulence are presumably more amenable to model as both the joint PDF and the conditional mean remain relatively scale-independent (after proper normalization). However, at $s = 6$, where $\ell_6 \approx 126\ell_k$ [Fig. 18(b)], Π_{SFS} and the particle number density are decorrelated (similar to $s = 4$ in Fig. 15), implying that a filter width $\ell_\Delta \gtrsim \ell_6$ renders the resolved flow motions SGS loaded even for these heavy particles.

Overall, the current study shows the complexity of LES modeling associated with two-way coupled point particles, and the importance of $\mathrm{St}_{\mathrm{SGS}}$ in designing the corresponding LES study. Physically consistent behavior of the SGS model and LES grid resolution should be considered simultaneously, and grid refinement (for flows laden with the critical particles) and coarsening (for those with high-Stokes particles) cannot be performed arbitrarily. The former case (with the critical particles) requires us to model the SGS effects on particle aerodynamics (as done comprehensively for one-way coupled setups), while the latter (with high-Stokes particles) does not. However, the latter case appears to call for the development of a new SGS closure that takes into account resolved particle concentration or an additional modeling of the resolved interphase coupling term Eq. (3).

VI. CONCLUDING REMARKS

Wavelet multiresolution analysis (WMRA) is developed for characterizing how inertial point particles dilutely suspended in decaying incompressible homogeneous isotropic turbulence modulate the interphase, cross-scale transfer of turbulence kinetic energy (TKE). The formulation is based on that of Meneveau [28] and extends the work of Bassenne *et al.* [33] for spectral energy transfer and two-way coupled particle-laden flow. Direct numerical simulation is performed for the carrier-phase turbulence, and inertial particles are simulated using the standard Euler-Lagrange formulation. The two phases are coupled via the Stokes drag law in two ways. A single-phase turbulence is simulated as a baseline case, and interactions between the carrier phase and monodispersive particles are examined at initial particle Stokes numbers $\mathrm{St}_{k,0} = 1$ and 10, respectively. At the critical Stokes number ($\mathrm{St}_k = 1$), the particle acceleration time is comparable to the Kolmogorov timescale. As a result, those particles tend to be ejected from regions of high vorticity and accumulated at high concentration forming filamentous clusters where local strain rate is high [1,11]. Aerodynamics of high-inertia particles is drastically different from that of the critical particles, and their spatial distribution is more uniform.

Although similar configurations have been studied previously by many others [18,19,40,41,44], the impact of particles on the momentum transfer of turbulence has been understood in the spectral space only, a restriction imposed by the Fourier analysis adopted by the previous studies. Thus, the spatially local nature of $\mathrm{St}_k = 1$ particle cluster has not been studied in detail with regard to their two-way interactions with the carrier-phase turbulence. Extending the work of Bassenne *et al.* [33] (based on Meneveau [28] for single-phase turbulence), interphase, cross-scale TKE transfer is characterized using the discrete wavelet transform and a multiresolution framework [39]. In particular, its dependence on particle inertia and concentration is examined. Scale-dependent joint wavelet statistics are used to decompose and correlate interphase, cross-scale interactions.

Interphase interactions estimated using wavelet statistics show close agreement with the previous studies based on the Fourier theory, particularly for heavy particles that are ballistic in nature and distributed more uniformly in space. They behave as average sinks of energy. It is also found that they are definite energy sinks at all scales and positions (not just on average) and directly suppress

turbulent motions. Thus, the standard energy cascade takes a secondary role in decaying the carrier-phase turbulence suspended with heavy particles.

Unlike heavy particles, the preferentially concentrated particles ($\mathrm{St}_k = 1$) are not definite sources or sinks of TKE. The Fourier theory (see, for instance, Ref. [19]) shows that they are sources at small scales and sinks at large scales, also confirmed by the present study for mean wavelet statistics. However, their spatially local interactions with the carrier phase are more complicated. Clusters of $\mathrm{St} = 1$ particles are characterized by the coexistence of particularly strong small-scale sources and sinks of TKE with similar probabilities. The cross-scale transfer of TKE (namely, downscale and upscale) is enhanced (downscale transfer, in particular). However, it is not considerably amplified by such clusters, and the subfilter-scale energy flux is much less intermittent than that of the baseline, single-phase turbulence, suggesting that the enhanced cross-scale transfer by the critical particles is more nonlocal in space. Overall, local particle concentration alone is not a distinct indicator for whether the critical particles amplify or extract TKE from the carrier phase or whether they contribute either forward or backward scatter of TKE. However, particle concentration appears to be correlated with interphase transfer (and also with cross-scale transfer) in such a way that their contributions to TKE should be modeled using a bimodal-like distribution. On the contrary, regions of negligibly small particle concentration (created by the preferential concentration) are well characterized by the neutral interphase and in-scale transfer.

With regard to subgrid-scale (SGS) modeling of two-way coupled particle-laden turbulence, this study provides several useful suggestions and questions. Unlike one-way coupled configurations (or highly diluted suspensions), applying SGS closures developed for single-phase turbulence should be done with care. Joint wavelet statistics examined in this study show distinct correlations involving interphase, interscale transport as a function of particle inertia. This study shows *a priori* that a design of large-eddy simulation (LES) of two-way coupled particle-laden turbulence should be done in such a way that such correlations should be retained, thus making LES physically consistent. For instance, that can be done by preserving the SGS Stokes number *a posteriori*, a more appropriate metric than the particle Stokes number itself. Using SGS models designed for particle-free simulations as they are should be restricted to setups where SGS loaded behavior dominates ($\mathrm{St}_{\mathrm{SGS}} \ll 1$). However, it should be noted that, due to the definition of $\mathrm{St}_{\mathrm{SGS}}$, such behavior may be altered by LES grid refinement. In the limit of $\mathrm{St}_{\mathrm{SGS}} \gg 1$, it appears that resolved particle concentration should be considered in evaluating SGS closure terms, and SGS energy transfer evaluated *a posteriori* should demonstrate a bimodal-like behavior, as the current *a priori* analysis suggests. For instance, the filtered two-way coupling term Eq. (3) can be a candidate through which such behavior is manifested.

Some of the findings in this study need further investigations with regard to the standard Euler-Lagrange formulation based on the particle-in-cell concept for its sensitivity to the numerical method and grid resolution. Related future works include grid sensitivity tests of wavelet statistics examined in Secs. IV and V. Relatively low local volume fractions and a particle Reynolds number that is much less than unity justify the use of the standard Stokes drag model. However, using a correction model by, for instance, Tenneti and Subramaniam [12] appears to be more relevant to turbulent flows laden with particles accumulating at a volume fraction of $O(10^{-1})$. In addition, the current average volume fraction 10^{-3} suggests to examine particle-particle collision effects for the critical particles in particular. In addition, it is interesting to incorporate several recently proposed algorithms for a two-way coupled Euler-Lagrange formulation [45–49] and assess (in conjunction with a grid sensitivity study) their impacts on interphase and interscale fluxes evaluated using WMRA.

It should be pointed out that the present study analyzes a decaying HIT which does not achieve a statistically stationary state and thus restricts the analysis to the early period of decay when the Stokes number remains approximately constant (see Fig. 3). Although several techniques [50,51] exist for generating statistically stationary two-way coupled HIT, their direct impacts on particle dispersion are not well understood. Besides, some of those artifacts could be transferred to the carrier phase via the two-way coupling. Studying a decaying turbulence allows us to exclude such

artifacts in describing interscale, interphase energy transfer. However, analyzing forced HIT or other stationary natural turbulence laden with inertial particles is certainly useful to strengthen the conclusions of the analysis, and this will be pursued in subsequent studies.

Some of the observations and conclusions made by this study could be a function of parameters such as the mass loading ratio, volume fraction, particle Stokes number, Reynolds number, and so forth. Thus, exploring the dependence of wavelet statistics on the range of those parameters is useful to further strengthen the arguments of this study. Finally, several discussions made regarding the joint wavelet statistics are rather qualitative. Thus, a proper quantifiable statistical metric can be useful to describe unambiguously interphase, cross-scale energy transfer as a function of particle inertia, turbulence intensity, and so forth.

ACKNOWLEDGMENTS

The authors are grateful to Javier Urzay for sharing useful discussions at the early phase of this study and providing important suggestions. M.N. and J.K. appreciate Hadi Pouransari for help regarding the numerical method used in the DNS code. M.N. and J.K. acknowledge fruitful discussions with Houssem Kasbaoui at Arizona State University.

[1] S. Balachandar and J. K. Eaton, Turbulent dispersed multiphase flow, Annu. Rev. Fluid Mech. **42**, 111 (2010).
[2] A. Y. Varaksin, *Turbulent Particle-laden Gas Flows* (Springer, Berlin, Heidelberg, 2007).
[3] A. Prosperetti and G. Tryggvason, *Computational Methods for Multiphase Flow* (Cambridge University Press, Cambridge, 2009).
[4] C. T. Crowe, J. D. Schwarzkopf, M. Sommerfeld, and Y. Tsuji, *Multiphase Flows with Droplets and Particles* (CRC, Boca Raton, FL, 2011).
[5] S. P. Arya *et al.*, *Air Pollution Meteorology and Dispersion* (Oxford University Press New York, 1999), Vol. 6.
[6] A. W. Woods, Turbulent plumes in nature, Annu. Rev. Fluid Mech. **42**, 391 (2010).
[7] D. Lewis and T. Pedley, Planktonic contact rates in homogeneous isotropic turbulence: Theoretical predictions and kinematic simulations, J. Theor. Biol. **205**, 377 (2000).
[8] M. Abkarian, S. Mendez, N. Xue, F. Yang, and H. A. Stone, Speech can produce jet-like transport relevant to asymptomatic spreading of virus, Proc. Natl. Acad. Sci. (USA) **117**, 25237 (2020).
[9] D. W. Rouson and J. K. Eaton, On the preferential concentration of solid particles in turbulent channel flow, J. Fluid Mech. **428**, 149 (2001).
[10] S. L. Post and J. Abraham, Modeling the outcome of drop–drop collisions in diesel sprays, Int. J. Multiphase Flow **28**, 997 (2002).
[11] M. R. Maxey and J. Riley, Equation of motion for a small rigid sphere in a turbulent fluid flow, Phys. Fluids **26**, 883 (1983).
[12] S. Tenneti and S. Subramaniam, Particle-resolved direct numerical simulation for gas-solid flow model development, Annu. Rev. Fluid Mech. **46**, 199 (2014).
[13] S. Subramaniam, Multiphase flows: Rich physics, challenging theory, and big simulations, Phys. Rev. Fluids **5**, 110520 (2020).
[14] J. G. Kuerten, Point-particle DNS and LES of particle-laden turbulent flow—a state-of-the-art review, Flow Turbul. Combust. **97**, 689 (2016).
[15] C. Marchioli, Large-eddy simulation of turbulent dispersed flows: a review of modelling approaches, Acta Mech. **228**, 741 (2017).
[16] C. Meneveau and J. Katz, Scale-invariance and turbulence models for large-eddy simulation, Annu. Rev. Fluid Mech. **32**, 1 (2000).

[17] J. Urzay, M. Bassenne, G. I. Park, and P. Moin, Characteristic regimes of subgrid-scale coupling in LES of particle-laden turbulent flows, *Annual Research Briefs* (Center for Turbulence Research, Stanford University, 2014), p. 3.
[18] K. D. Squires and J. K. Eaton, Particle response and turbulence modification in isotropic turbulence, Phys. Fluids **2**, 1191 (1990).
[19] A. Ferrante and S. Elghobashi, On the physical mechanisms of two-way coupling in particle-laden isotropic turbulence, Phys. Fluids **15**, 315 (2003).
[20] A. H. Abdelsamie and C. Lee, Decaying versus stationary turbulence in particle-laden isotropic turbulence: Heavy particle statistics modifications, Phys. Fluids **25**, 033303 (2013).
[21] G. Wang and D. H. Richter, Two mechanisms of modulation of very-large-scale motions by inertial particles in open channel flow, J. Fluid Mech. **868**, 538 (2019).
[22] M. Farge, Wavelet transforms and their applications to turbulence, Annu. Rev. Fluid Mech. **24**, 395 (1992).
[23] K. Schneider and O. V. Vasilyev, Wavelet methods in computational fluid dynamics, Annu. Rev. Fluid Mech. **42**, 473 (2010).
[24] M. Farge and K. Schneider, Wavelet transforms and their applications to MHD and plasma turbulence: a review, J. Plasma Phys. **81**, 435810602 (2015).
[25] J. G. Brasseur and Q. Wang, Structural evolution of intermittency and anisotropy at different scales analyzed using three-dimensional wavelet transforms, Phys. Fluids **4**, 2538 (1992).
[26] R. Camussi and G. Guj, Orthonormal wavelet decomposition of turbulent flows: Intermittency and coherent structures, J. Fluid Mech. **348**, 177 (1997).
[27] W. J. Baars, K. M. Talluru, N. Hutchins, and I. Marusic, Wavelet analysis of wall turbulence to study large-scale modulation of small scales, Exp. Fluids **56**, 188 (2015).
[28] C. Meneveau, Analysis of turbulence in the orthonormal wavelet representation, J. Fluid Mech. **232**, 469 (1991).
[29] S. G. Mallat, A theory for multiresolution signal decomposition: The wavelet representation, IEEE Trans. Pattern Anal. **11**, 674 (1989).
[30] D. C. Dunn and J. F. Morrison, Anisotropy and energy flux in wall turbulence, J. Fluid Mech. **491**, 353 (2003).
[31] J. Kim, M. Bassenne, C. A. Z. Towery, P. E. Hamlington, A. Y. Poludnenko, and J. Urzay, Spatially localized multi-scale energy transfer in turbulent premixed combustion, J. Fluid Mech. **848**, 78 (2018).
[32] A. Freund and A. Ferrante, Wavelet-spectral analysis of droplet-laden isotropic turbulence, J. Fluid Mech. **875**, 914 (2019).
[33] M. Bassenne, P. Moin, and J. Urzay, Wavelet multiresolution analysis of particle-laden turbulence, Phys. Rev. Fluids **3**, 084304 (2018).
[34] H. Pouransari, M. Mortazavi, and A. Mani, Parallel variable-density particle-laden turbulence simulation, *Annual Research Briefs* (Center for Turbulence Research, Stanford University, 2015).
[35] T. Passot and A. Pouquet, Numerical simulation of compressible homogeneous flows in the turbulent regime, J. Fluid Mech. **181**, 441 (1987).
[36] M. Bassenne, J. Urzay, G. I. Park, and P. Moin, Constant-energetics physical-space forcing methods for improved convergence to homogeneous-isotropic turbulence with application to particle-laden flows, Phys. Fluids **28**, 035114 (2016).
[37] S. Tenneti, R. Garg, and S. Subramaniam, Drag law for monodisperse gas–solid systems using particle-resolved direct numerical simulation of flow past fixed assemblies of spheres, Int. J. Multiphase Flow **37**, 1072 (2011).
[38] J. Urzay, A. Doostmohammadi, and J. M. Yeomans, Multi-scale statistics of turbulence motorized by active matter, J. Fluid Mech. **822**, 762 (2017).
[39] S. Mallat, *A Wavelet Tour of Signal Processing* (Elsevier, Amsterdam, 1999).
[40] S. Elghobashi and G. C. Truesdell, On the two-way interaction between homogeneous turbulence and dispersed solid particles. I: Turbulence modification, Phys. Fluids **5**, 1790 (1993).
[41] A. H. Abdelsamie and C. Lee, Decaying versus stationary turbulence in particle-laden isotropic turbulence: Turbulence modulation mechanism, Phys. Fluids **24**, 015106 (2012).
[42] H. Aluie, Scale decomposition in compressible turbulence, Physica D **247**, 54 (2013).

[43] G. I. Park, M. Bassenne, J. Urzay, and P. Moin, A simple dynamic subgrid-scale model for LES of particle-laden turbulence, Phys. Rev. Fluids **2**, 044301 (2017).
[44] A. M. Ahmed and S. Elghobashi, On the mechanisms of modifying the structure of turbulent homogeneous shear flows by dispersed particles, Phys. Fluids **12**, 2906 (2000).
[45] P. Gualtieri, F. Picano, G. Sardina, and C. M. Casciola, Exact regularized point particle method for multiphase flows in the two-way coupling regime, J. Fluid Mech. **773**, 520 (2015).
[46] J. A. K. Horwitz and A. Mani, Accurate calculation of Stokes drag for point-particle tracking in two-way coupled flows, J. Comput. Phys. **318**, 85 (2016).
[47] P. J. Ireland and O. Desjardins, Improving particle drag predictions in Euler-Lagrange simulations with two-way coupling, J. Comput. Phys. **338**, 405 (2017).
[48] M. Esmaily and J. A. K. Horwitz, A correction scheme for two-way coupled point-particle simulations on anisotropic grids, J. Comput. Phys. **375**, 960 (2018).
[49] S. Balachandar, K. Liu, and M. Lakhote, Self-induced velocity correction for improved drag estimation in Euler–Lagrange point-particle simulations, J. Comput. Phys. **376**, 160 (2019).
[50] G. Mallouppas, W. K. George, and B. G. M. van Wachem, New forcing scheme to sustain particle-laden homogeneous and isotropic turbulence, Phys. Fluids **25**, 083304 (2013).
[51] Y. Yao and J. Capecelatro, Deagglomeration of cohesive particles by turbulence, J. Fluid Mech. **911**, A10 (2021).